Geophysics Open File Report No. 24
Geoscience Department
New Mexico Tech
Socorro, NM 87801

MICROEARTHQUAKE FREQUENCY ATTENUATION OF S PHASES IN THE RIO GRANDE RIFT NEAR SOCORRO, NEW MEXICO

by

James A. Johnston

Submitted in partial
fulfillment
of
the requirements
for
Geophysics 590
and the
Master's Degree Program
at
New Mexico Institute
of
Mining and Technology

May, 1978

The research described in this paper was sponsored jointly by the National Science Foundation (Grants DES74-24187 and EAR77-23166) and the New Mexico Energy Institute - New Mexico State University (Grants EI-176-032 and EI-177-083).

ABSTRACT

Arrays of 5 to 9 portable, high-gain (~10^6 magnification at 40 Hz) seismographs were used to record microearthquakes from April, 1975, through January, 1978, in the vicinity of Socorro, New Mexico. Eight volumes in the crust have been proposed to explain anomalous absorption of the higher frequencies of S waves in the recorded microearthquakes. Crustal volumes with anomalous attenuation were defined by intersecting raypaths, along which unusual high frequency S wave absorption was observed. The degree of absorption was determined by measuring the dominant frequency of the S wave using a zero-crossing counting technique and relating this quantity to Q, the quality factor. Approximately 5 percent of the raypaths examined showed anomalous S wave frequency attenuation.

Five possible mechanisms for the anomalous absorption were considered (1) variation of source parameters, (2) spectra variation with change in azimuth around the focus, (3) normal absorption for raypaths traversing large distances, (4) station effects, and (5) raypath travel through an anomalous crustal volume. The effects of the first four mechanisms are shown to be minimal. Partial melts, heated rock, or fluid-filled microfractures could explain the fifth mechanism. Heated rock appears to be the most likely explanation for the observations.

Three crustal volumes are defined which are most likely to be associated with magmatic intrusion (1) the region ~3.5 km ESE of station WT, in the Socorro Basin (depth: ~3.2 km), (2) the region ~3.0 km NW of station WM in the southeast of the La Jencia Basin (depth: ~4.6 km), and (3) the region ~2.5 km NE of station SC in the southwest of the La Jencia Basin (depth: ~4.1 km). The depths given are the shallowest

points of the anomalous crustal volumes.

The relation $Q_\alpha/Q_\beta = \nu_\alpha/\nu_\beta$ is proposed (ν = dominant frequency, α and β refer to P and S waves, respectively). The normal, unattenuated value of Q_α/Q_β for the Socorro area is observed to be 1.60. The mean values for the three anomalous volumes described above, as calculated from the Q_α/Q_β ratios associated with the raypaths defining the volumes, are (1) 2.76, (2) 2.71, and (3) 2.29. The higher the ratio the greater the absorption. The higher ratios are all attributable to an increase in the absorption of S wave energy.

INTRODUCTION

Microearthquakes have been recorded regularly in the Socorro area since June 1960. In the past few years these events have been used to investigate the presence of magma at intermediate depths beneath the Rio Grande rift. Several geophysical observations have led researchers to believe that an extensive (~1700 km^2) layer of magma exists at depths of 18 to 20 km (1) diffuse geographical distribution of seismic activity, (2) unusually strong S to P (S_xP) and S to S (S_xS) reflections, (3) high heat flow, and (4) historical surface uplift (Sanford et al., 1976). In addition to these investigations research is presently being conducted to attempt to identify the spatial extent of shallower (<13 km) magma bodies whose source could be the deeper magma layer. Such research is the goal of the study described in this report.

The purpose of this investigation was to map the volumes of crust defined by intersecting raypaths along which frequency attenuation in the S wave of microearthquakes was observed. Assuming such attenuation to be due to heated rock the crustal volumes so defined should approximately locate volumes affected by partial melts at greater depths. Previous

related studies include (1) Shuleski (1976), (2) Sanford (1977), (3) Matumoto (1971), and (4) Kubota and Berg (1968). All these studies involve the mapping of intersecting raypaths along which screening, or nearly complete screening, of the S wave of microearthquakes is observed. In particular, Shuleski (1976) performed a complete analysis of fault plane solutions and angles of incidence in the Socorro area and determined that only 38 percent of the weak or missing S waves could be explained by these factors. The remaining 62 percent he attributed to screening by magma bodies.

Figures 1 and 2 are presentations of the results of Shuleski (1976) as modified by Sanford (1977). The lines represent raypaths, drawn from hypocenters to the stations at which screening was observed. Ratios of P wave to S wave amplitudes are plotted to indicate the degree of screening. These ratios eliminate problems resulting from differences in strength of microearthquakes and distances to recording stations (Shuleski, 1976). The tentative locations for four magma bodies are outlined; when dashed lines are used the location is not well known. The numbered points, lying along the axes of the outlined regions, are depths calculated to raypaths crossing the axes of the regions.

The basic measurement in this study was the counting of the number of zero-crossings observed in the S wave. This was then converted to dominant frequency. Microearthquake data were obtained from April 1975 to January 1978 using a moveable array of 5 to 9 seismograph stations. Considerable effort was made to obtain accurate hypocenter locations as the accuracy of the final placement of the anamolous volumes depended on correct raypath plotting.

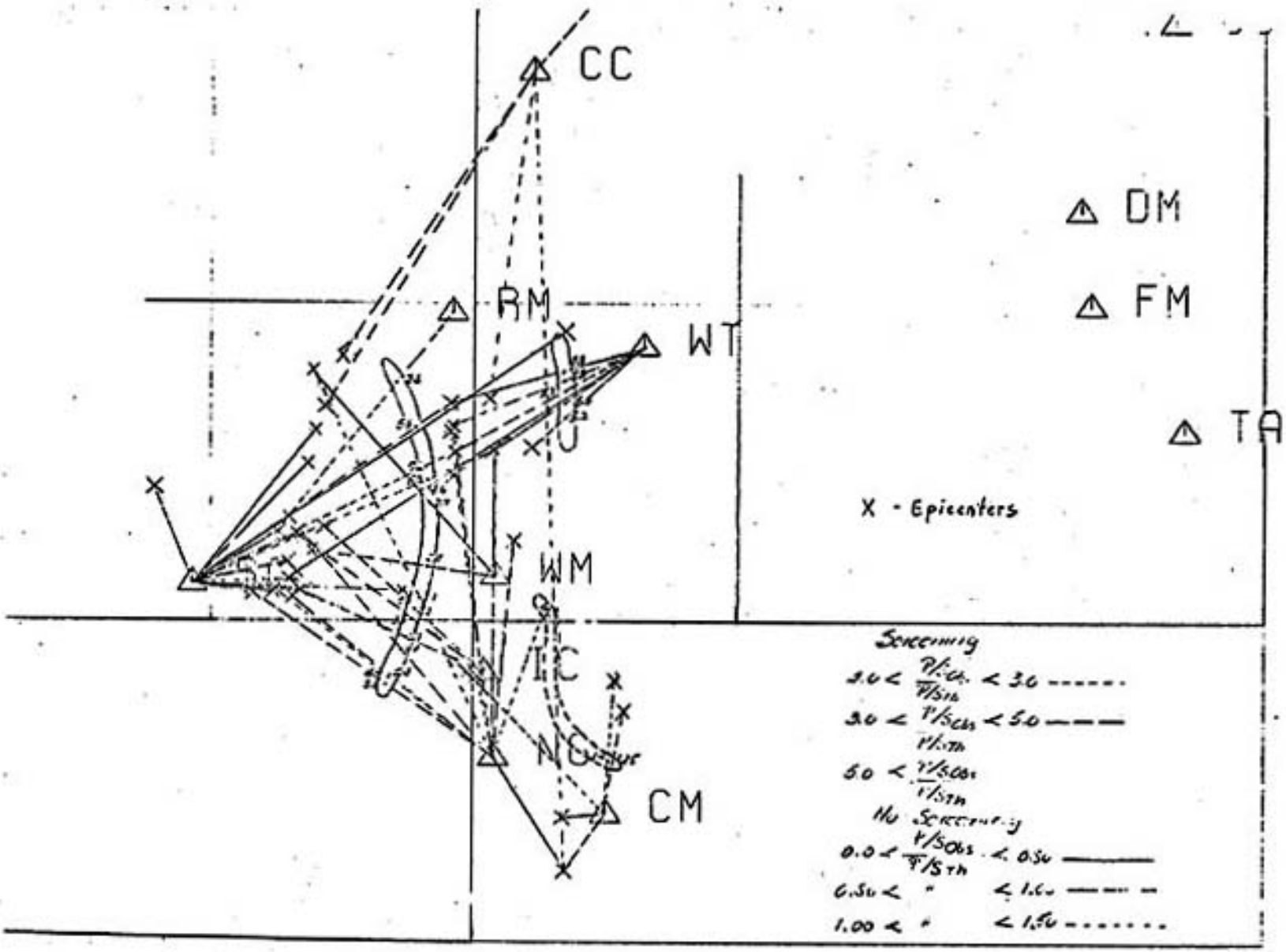

Figure 1. The S wave screening data of Shuleski (1976), as modified by Sanford (1977).

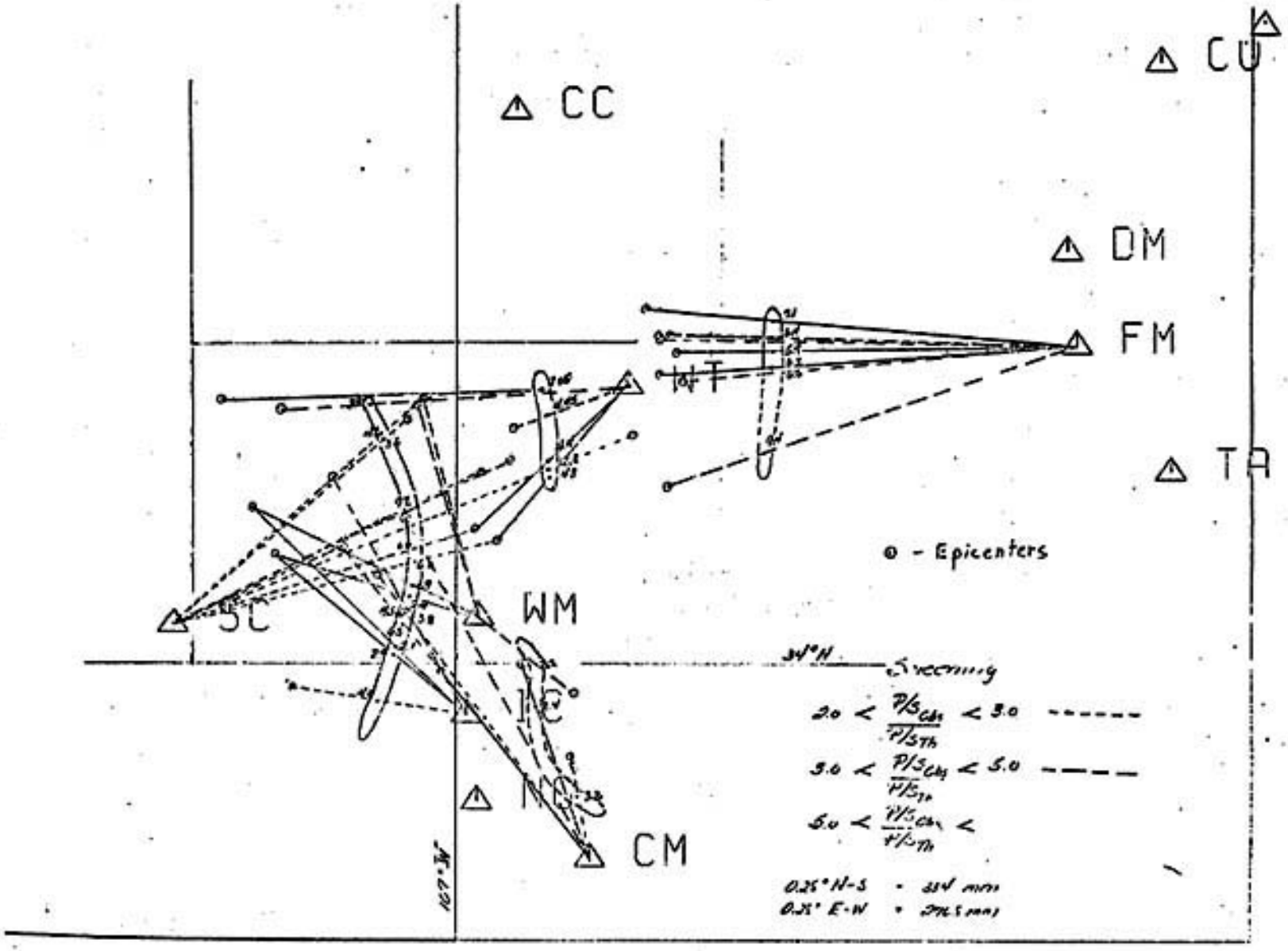

Figure 2. The S wave screening data of Shuleski (1976), as modified by Sanford (1977).

GEOLOGICAL SETTING

The area of investigation is located within the Rio Grande rift approximately 125 km south of Albuquerque. The rift is a major extensional structure formed by east-west tension beginning about 25 to 29 m.y. ago and continuing to the present (Chapin and Seager, 1975). The rift extends from southern New Mexico into central Colorado and consists of a series of interrelated structural depressions with raised margins having a general northern trend. The rift penetrates the Southern Rocky Mountains of northern New Mexico and southern Colorado, lies between the Colorado Plateau and High Plains in central New Mexico, and merges to the south in a complicated manner with the Basin and Range province. Approximately 50 km north to 30 km south of Socorro the rift is further modified by intergraben horsts believed to be only 9 to 10 m.y. old, suggesting a recent crustal structural anomaly (Chapin and Seager, 1975). The map shown in Figure 3 illustrates the general physiographic features and locations of stations utilized in this study. Intergraben horsts shown are the Socorro-Lemitar and Chupadera mountains, separating the La Jencia and Socorro basins.

A large amount of evidence indicates that volcanic activity accompanied formation of the rift. The most active periods appear to have been from 20 to 26 m.y. ago and from 5 m.y. ago to the present (Chapin and Seager, 1975). The first period of volcanism has basaltic andesites associated with it, while true basalts dominate the flows of very recent age in the Socorro area.

A ribbon of high heat flow (>2.5 HFU) is roughly coincident with a number of thermal springs occurring along the western margin of the rift (Reiter et al., 1975), the hottest and largest of which are located in

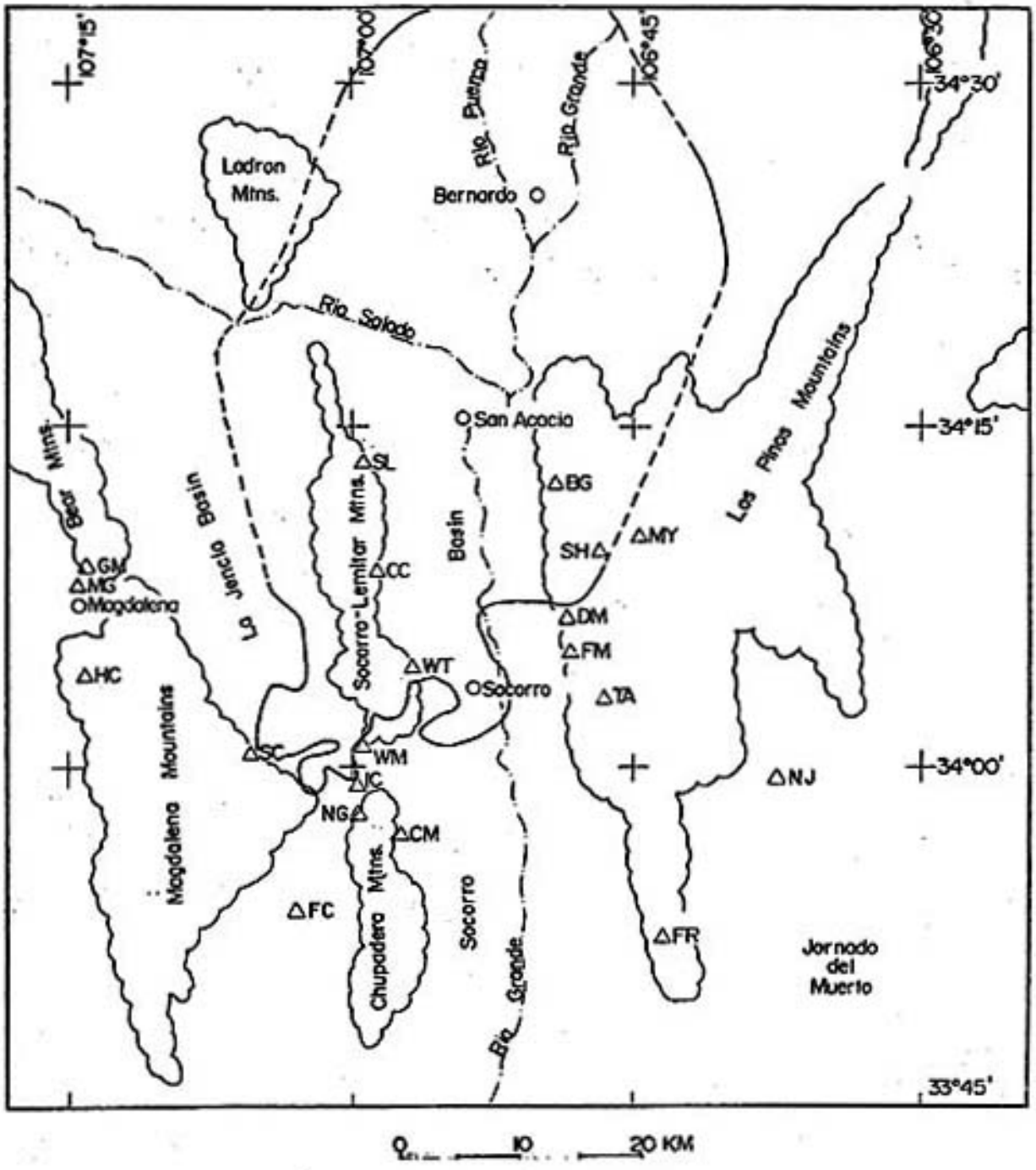

Figure 3. Physiographic features of the Socorro area, seismic station locations, and outline of the deep (18 km) magma body (from Sanford, and others, 1977).

the southern end of the Socorro-Lemitar mountains. This is also an area of very high heat flow (Sanford et al., 1977).

The outline of the deep, extensive magma body located between 18 and 20 km in depth is shown in Figure 3. Dotted lines indicate boundaries where more data is required to map them accurately. The shape of the body appears to be a thin, elongate sill having a general north-south trend with its axis following beneath the Socorro-Lemitar mountain block. The minimum depth to the body of 18 km is located beneath Socorro Mountain. It deepens to approximately 20 km along the margins (Rinehart, 1976). The body dips northward approximately 6° (Sanford, Alptekin, and Toppozada, 1973).

INSTRUMENTATION

Two basic types of portable seismic systems were employed throughout the data collection period. For the interval April 1975 through January 1978, an array of 5 to 6 Sprengnether MEQ-800 analog recording units was deployed. This basic array was supplemented, starting in April, 1977, with two Sprengnether DR-100 digital recording units. In addition to these units a Kinematics PS-1 analog unit was used to record station LAD which is telemetered via telephone line directly to the campus of New Mexico Institute of Mining and Technology. The MEQ-800 seismographs served as the primary source for the data. The DR-100 systems were mainly used to improve hypocenter locations by expanding and better defining the arrays. They were also used to determine the dominant frequencies of unattenuated P and S phases because they produced the best high-resolution records.

From April, 1975 to September, 1977 most of the arrays were deployed in the southern part of the area shown in Figure 3 (roughly south of

34°05'N). From September, 1977 to January, 1978, the arrays were to the north (between 34°08'N and 34°30'N). However most of the data collected was from the south and thus this study is primarily concerned with that area.

The MEQ-800 seismic system records helically on a drum covered with smoked paper at a speed of 120 ± 0.6 mm/min. The gain stable amplifier has settings ranging from 60 to 140 db in discrete 6 db intervals. The most common settings used in the field were 84 and 90 db. Both low and high frequency filters were available. The low frequency filter was always set at Out and the high frequency filter was set at either Out or 30 Hz. The high frequency 30 Hz setting attenuated frequencies higher than 30 Hz, but did not seriously affect the response of the system to the dominant frequencies observed in microearthquakes (P wave < 30 Hz). Magnification response cruves for the system at both settings of the high frequency filter, Out and 30 Hz, are shown in Figure 4 for both the Willmore vertical component (1.5 Hz natural frequency) and Mark-Products L4-C vertical component (1.0 Hz natural frequency) seismometers.

Each MEQ-800 has a quartz crystal chronometer which produces time marks on the record at one minute intervals. The chronometers were synchronized at the beginning of each recording week with a time signal from WWV and were checked for drift at the end of the week in the same manner. The recording week generally started Monday morning and the units were retrieved Friday afternoon. During this time period the chronometer drift was assumed to be linear. This has been verified by trial runs of the units in which twice-daily checks were made under field conditions with the time signal from WWV. The maximum variation from linearity found was approximately 0.03 sec, but most of the time the variation was

much less than this. The linear drift observed was always less than 0.10 sec/day.

The two DR-100 units record digitally on magnetic tape cassettes at a sampling rate of 100/sec. The amplifier gains were set at discrete 6 db intervals in the range 78 to 96 db. The filters were set at High-Out and Low-Out the entire time the units were in the field.

The seismometers for the DR-100 units were Mark-Products L4-C vertical component geophones. A Sprengnether DP-100 tape playback unit and Beckman Dynograph strip-chart recorder were used to obtain analog records from the digital magnetic tapes. The strip-chart recorder produced an ink on paper record with a wide variety of playback speeds possible.

Listed in Table 1 are the locations of the seismic stations occupied during this study.

DATA ACQUISITION AND REDUCTION

Almost all of the primary data collected for this study (the counting of zero-crossings in S waves) were taken from the MEQ-800 records. The entire set of records, from April, 1975 to January, 1978, was first scanned by eye to pick out events that appeared to have attenuation of high frequencies in the S wave but not in the P phase. In doing this a 'whiteout' criterion was used to make a rapid determination of this type of attenuation. The recording pen leaves a white trace on the smoked paper as the microearthquake signature is written. At high frequencies, individual, adjacent cycles are indiscernable and the trace leaves a band of white. This is the definition of 'whiteout' and photographic examples are presented in Plate 1. However, at lower dominant frequencies individual cycles can be resolved and the zero-crossings counted. From

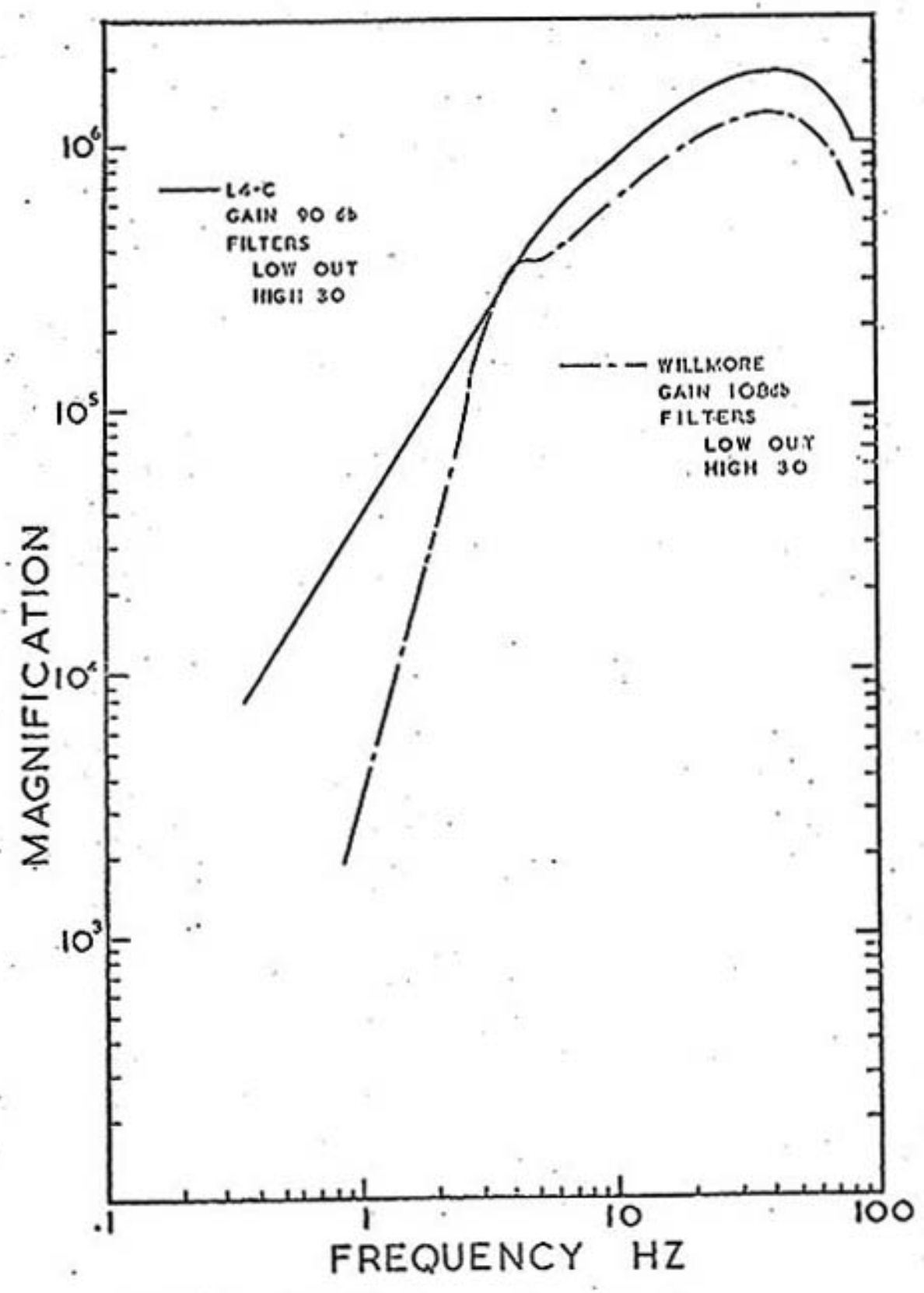

Figure 4a. Magnification response curves for the MEQ-800 seismographs. The high-frequency filter is set in the 30 Hz position (adapted from Rinehart, 1976).

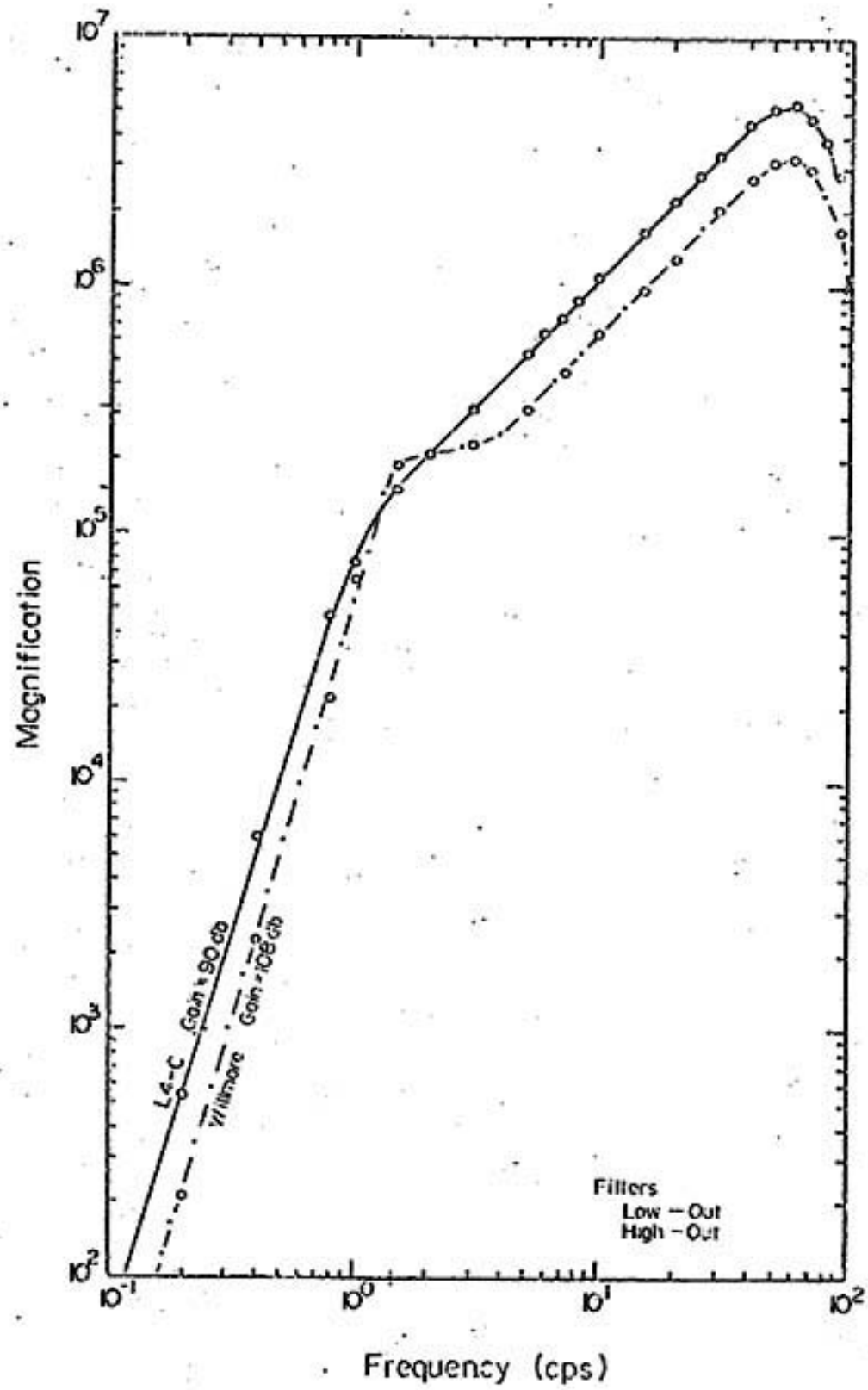

Figure 4b. Magnification response curves for the MEQ-800 seismographs. The high-frequency filter is set in the Out position (from Shuleski, 1976).

Table 1. Location of Seismic Stations

Station	Latitude	Longitude	Elevation (m)
BG	34.2068	106.8205	1516
CC	34.1442	106.9812	1649
CM	33.9501	106.9576	1640
CU	34.1573	106.7785	1585
DM	34.1075	106.8079	1536
FM	34.0829	106.8047	1537
HC	34.0658	107.2361	2240
IC	33.9870	106.9967	1730
LAD	34.4583	107.0375	1768
LPM	34.3076	106.6336	1737
MG	34.1305	107.2425	2024
MY	34.1667	106.7459	1645
NJ	33.9924	106.6253	1644
SC	34.0100	107.0894	2073
SL	34.2234	106.9910	1615
TA	34.0498	106.7751	1558
WM	34.0120	106.9929	1673
WT	34.0722	106.9459	1555
GM	34.1454	107.2345	1945
RI	34.4234	107.2075	1530
CK	34.2725	106.7702	1578
BB	34.4090	106.6818	1615
PC	33.8950	107.0504	1850

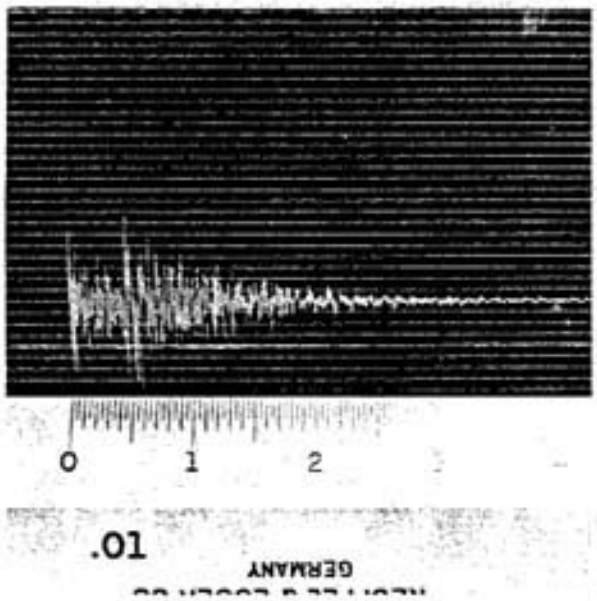

AUGUST 12,1975 MY
7:09 UST

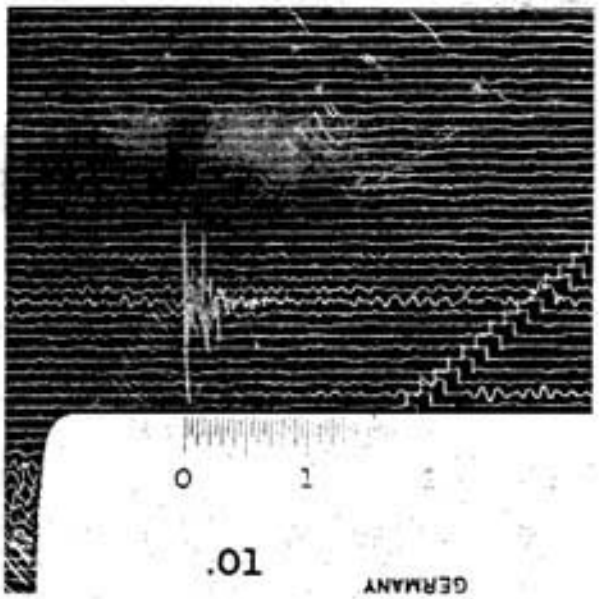

JUNE 3,1975 FM
9:38 UST

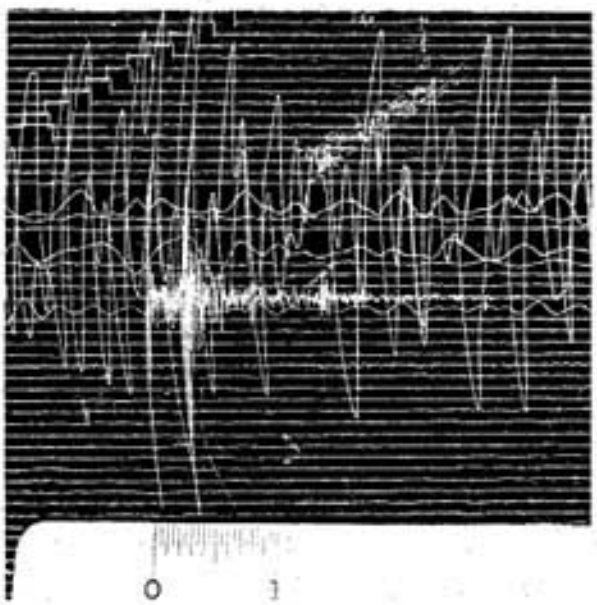

JUNE 3,1975 SC
15:10 UST

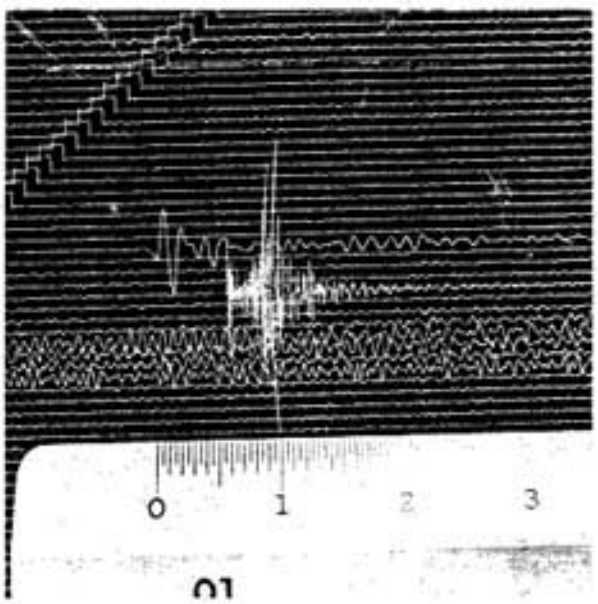

MAY 29,1975 CM
7:14 UST

Plate 1. Examples of events in which the P and S waves are unattenuated.

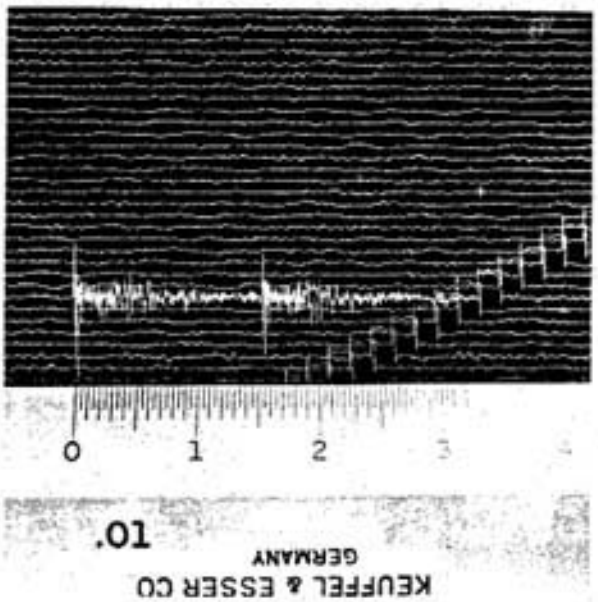

AUGUST 25, 1975 FM
19:37 UST

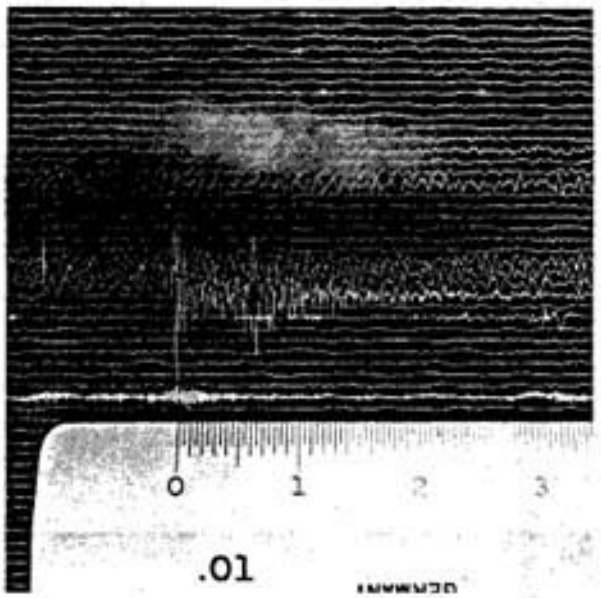

JANUARY 23, 1976 DM
2:53 UST

JANUARY 21, 1976 CM
14:18 UST

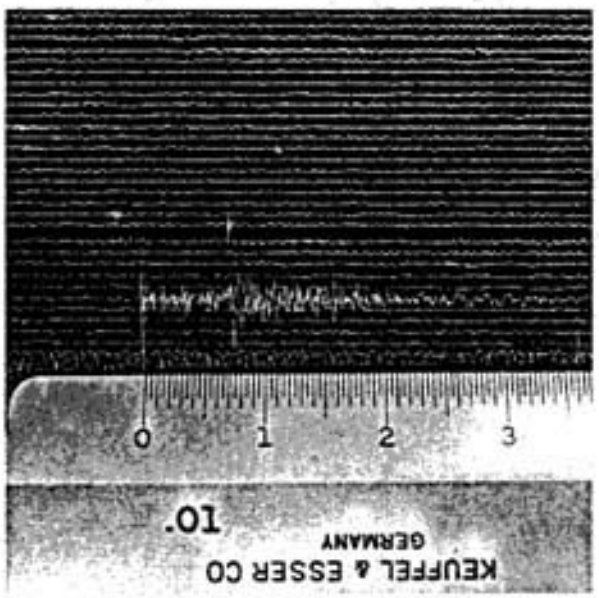

AUGUST 17, 1977 DM
2:20 UST

Plate 2. Examples of events in which the P wave is unattenuated, but the S wave shows loss of high frequencies.

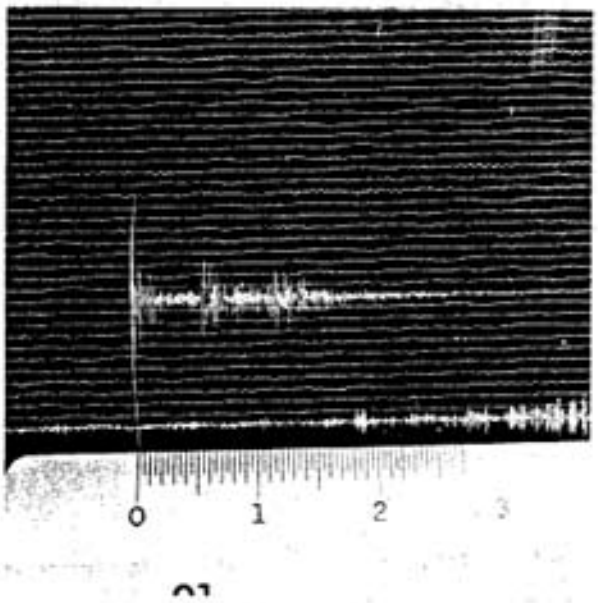

SEPTEMBER 2,1977 CC
13:29 UST

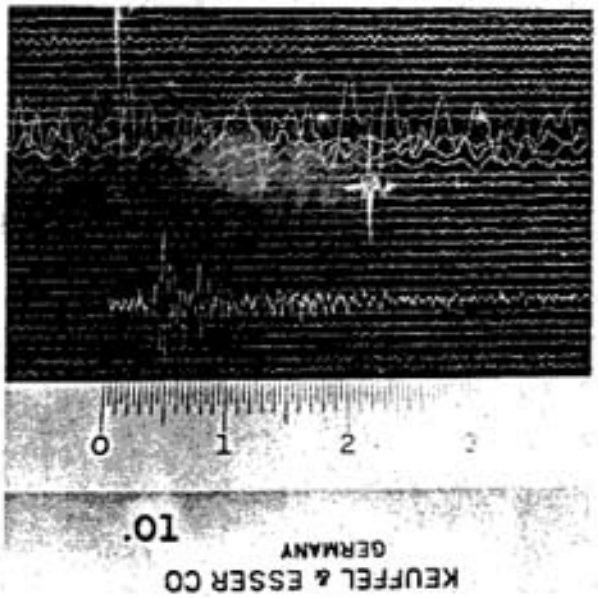

JANUARY 23,1976 CM
7:22 UST

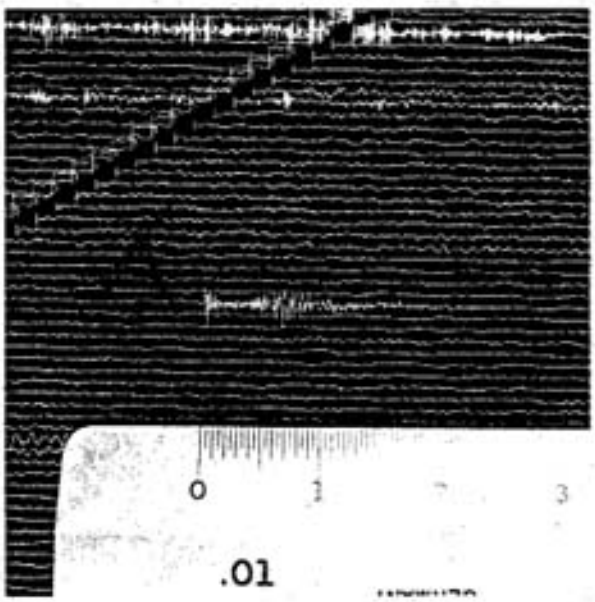

OCTOBER 8,1976 DM
00:21 UST

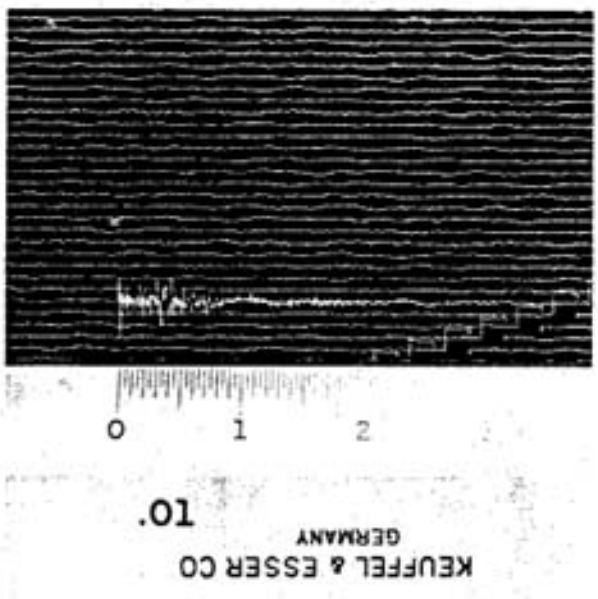

FEBRUARY 10,1977 DM
7:33 UST

Plate 2. (Continued)

measurements on records approaching this limit, it was found that the lower frequency range in which whiteout was still observed was approximately 12 to 18 Hz. This frequency range was a function of trace thickness and general background noise. In general, resolution on most records was quite good and frequencies in the range of interest for this study were readily obtained by the zero-crossing counting technique. Thus, when first scanning the records by eye, events were chosen in which the P phase showed 'whiteout' and the S phase exhibited easily counted zero crossings. Examples of events meeting these criteria are shown in the photographs of Plate 2.

After the initial selection and location of the attenuated event, the zero crossings were converted to dominant frequency using the relation,

$$\nu = \frac{n-1}{2} \quad , \tag{1}$$

where n is the number of zero crossings. The zero reference was defined by extending the line of the undisturbed seismic trace preceeding the event across the signature of the P and S phases through the coda.

The final result of this event selection process was a group of 83 microearthquake events in which the P phase appeared relatively unattenuated but the S wave showed an unusually low dominant frequency. The total number of events examined was approximately 320. Assuming an average of 5 raypaths per event, about 5 percent of the raypaths examined showed an unusually low dominant S wave frequency.

Two types of computer location routines were employed to determine the placement of the hypocenters. The first was an iterative numerical inversion method in which an initial estimate of the location and origin time were input along with the times of the direct P arrivals at each

of the stations in the array. The initial estimate for the origin time was taken from a Wadati plot and the initial epicenter location was determined from intersecting arcs whose radii were based on S-P times obtained from the records at each station in the array. An initial depth estimate of 7.0 km was usually made. Depth was the least well determined parameter. Kinehart (1976) gives a detailed account of the location procedure and errors involved.

After an acceptable location was obtained from the iterative routine the resulting origin time, along with the measured P arrival times, were used in a computer adaptation of the graphical procedure of intersecting hemispheres described by Richter (1958). This program produced a map of intersecting circles. Chords were drawn between the intersection points of the circles and the middle of the area defined by the intersection of these chords established the epicenter. The tightness of the cluster of intersecting chords indicated the quality of the solution. If the chords intersected at nearly the same point, the solution was considered good and no further modifications were made. If there was a large spread in the intersection of the chords, the origin time was allowed to vary within 0.5 seconds of the Wadati origin time until the tightest cluster of chord intersections was obtained. Usually the solution obtained in this manner was very close to the location produced by the iterative inversion program.

All the microearthquakes used in this study were located once following the above procedure. They were then located a second time using the locations obtained the first time as initial estimates. New station corrections, discussed below, and, in some cases, new direct P arrival times, were used in the second locations. The results from these second

locations were then used in the study. Only the iterative, numerical inversion routine was used for the second locations.

Corrections applied to the P arrival times prior to insertion in the location programs were (1) clock drift, and (2) station corrections. The clock drift for the four day recording week was assumed to be linear and separate drift curves were constructed every week for each unit in the field. Station corrections were estimated by carefully measuring arrival times of explosions whose locations and origin times were accurately known (Sanford, personal communication). Differences between theoretical and observed travel times for these explosions were attributed to effects of the geological column immediately beneath each station. Once accurate corrections were known for five or more stations in the array, other stations without corrections could be added to the array one at a time and run through the iterative inversion routine. Residuals obtained at the added station for a number of microearthquake events were then used to determine a station correction for the added station. Station corrections obtained from explosion data and the iterative technique are listed in Table 2.

Hypocenters were considered acceptable if (1) residuals calculated by the iterative inversion program were approximately equal to the timing error (0.05 sec), (2) error bars calculated by the program were of the order of the weighting used for each parameter (~1 km for longitude and latitude, ~3 km for depth and ~0.3 sec for the origin time), and (3) standard deviations, as calculated by the program, were less than ~0.06. Hypocenter locations meeting these criteria are listed in Table 3 along with the best estimate of the error bars associated with each parameter. The events in Table 3 constitute the data set used in this study. Of

Table 2. Station Corrections.

Station	Correction	Method of Determination
WT	0.00	explosion
CC	-0.11	
SL	-0.11	
GM	-0.11	
IC	-0.38	
RM	-0.44	
NG	-0.35	
CM	-0.42	
SC	-0.48	
DM	-0.11	
FM	-0.22	
BG	-0.22	
CU	-0.17	
WM	-0.32	
RI	-0.38	iterative inversion
MY	-0.12	
HC	-0.33	
FC	-0.47	
TS	-0.47	
TA	-0.15	
BB	-0.18	
CK	-0.22	

Table 3. Acceptable Hypocenter Locations.

Date		Origin Time	Error (sec)	Latitude	Error (km)	Longitude	Error (km)	Depth	Error (km)
*5-22-75	(2)	11:36:28.59	0.18	33.9135	1.15	106.9572	0.34	3.6	0.67
7-30-75	(34)	21:44:41.40	0.17	34.0760	0.38	106.9236	0.30	12.7	1.19
8-8-75	(31)	10:53:57.55	0.12	34.0482	0.49	106.9194	0.28	9.6	0.99
8-19-75	(26)	8:11:46.27	0.15	34.0440	0.28	106.9698	0.30	11.5	1.18
*8-19-75	(3)	10:00: 5.85	0.46	33.9551	1.23	107.0249	0.76	15.2	2.67
8-20/75	(33)	12:20:51.25	0.19	34.0749	0.40	106.9123	0.32	13.6	1.31
8-25-75	(32)	19:37:40.23	0.15	34.0682	0.35	106.9194	0.29	11.8	1.13
9-19-75	(13)	8:42:57.19	0.08	34.0032	0.40	106.8620	0.20	7.7	0.95
11-5-75	(48)	14.35: 4.24	0.38	34.0090	0.64	107.0956	1.45	13.4	2.10
11-7-75	(22)	13:52:34.77	0.18	34.0251	0.37	107.0930	1.76	6.3	1.09
1-21-76	(4)	14:18:27.96	0.20	33.9587	0.86	106.9595	0.32	8.5	1.31
1-23-76	(16)	2:53:32.71	0.29	34.0076	0.50	107.0418	0.76	10.8	1.97
1-23-76	(28)	7:22:14.37	0.19	34.0499	0.45	107.0470	0.65	6.1	1.65
1-27-76	(38)	8:37:43.36	0.53	34.1542	1.45	106.7963	1.33	15.7	2.92
1-29-76	(7)	18:24:27.27	0.16	33.9676	0.65	106.9899	0.31	8.5	1.16
4-13-76	(6)	11:58:34.35	0.12	33.9760	0.41	106.9713	0.35	6.5	0.79
4-16-76	(29)	9:33:42.54	0.15	34.0565	0.23	107.0212	0.34	7.8	1.20
4-20-76	(27)	2:52:19.50	0.36	34.0456	1.26	107.0705	1.47	9.0	1.14
*4-20-76	(36)	8:32:19.18	0.17	34.1069	0.57	106.8428	0.46	3.4	1.96
4-23-76	(8)	5:57:59.16	0.42	34.0327	1.60	107.0787	1.77	9.7	1.27
8-10-76	(19)	4:38:25.70	0.08	34.0109	0.45	107.0629	0.22	5.6	0.74
*10-6-76	(35)	15:12:40.83	0.33	34.0778	0.67	106.8017	1.32	13.4	1.76
10-7-76	(17)	23:21: 9.70	0.16	34.0076	0.86	107.0367	0.23	9.8	1.12
2-9-77	(20)	10:59:58.59	0.26	34.0173	0.56	107.0012	0.48	6.3	2.69
2-10-77	(37)	7:33:28.25	0.25	34.1230	0.95	106.9262	0.25	4.0	3.19
4-15-77	(24)	6:35:36.68	0.12	34.0371	0.57	107.0637	0.35	8.9	1.15
4-27-77	(18)	12:15:56.23	0.10	34.0011	0.48	107.0643	0.27	8.4	0.73
4-27-77	(21)	12:23:27.18	0.08	34.0178	0.33	107.0575	0.23	7.5	0.75
6-2-77	(9)	6:50:24.20	0.09	33.9993	0.46	107.0665	0.27	7.4	0.69
6-3-77	(14)	3:49: 1.35	0.09	34.0065	0.45	107.0619	0.26	7.8	0.72
6-3-77	(43)	20:45: 2.77	0.16	34.2284	0.47	106.8973	0.47	10.9	1.95

Table 3. Continued

Date		Origin Time	Error (sec)	Latitude	Error (km)	Longitude	Error (km)	Depth	Error (km)
*6-3-77	(5)	23:01:18.86	0.15	33.9717	0.65	107.0086	0.29	8.5	1.19
7-14-77	(39)	10:00:32.48	0.05	34.1602	0.19	106.8688	0.19	7.3	0.58
7-14-77	(23)	20:24:16.50	0.09	34.0347	0.31	107.0523	0.22	9.1	0.79
7-19-77	(42)	6:16:54.87	0.10	34.1581	0.37	106.8744	0.29	4.1	1.54
8-17-77	(44)	2:20:20.18	0.13	34.2877	0.23	107.0506	0.27	11.0	1.86
8-18-77	(40)	9:30:13.35	0.10	34.1609	0.30	106.8760	0.26	4.8	1.28
8-19-77	(15)	9:28:22.57	0.12	34.0072	0.55	107.0675	0.31	9.6	0.92
8-24-77	(10)	11:22:35.40	0.11	34.0009	0.43	107.0539	0.28	9.8	0.87
9-1-77	(30)	18:20: 2.29	0.14	34.0582	0.32	106.7625	0.69	8.3	1.19
9-1-77	(11)	21:58:48.35	0.12	34.0025	0.45	107.0415	0.27	9.9	0.98
9-2-77	(45)	13:29:30.83	0.38	34.3206	1.46	106.7799	1.34	15.3	1.38
9-20-77	(25)	1:20: 8.62	0.10	34.0376	0.55	107.0509	0.23	10.4	0.85
9-21-77	(41)	6:19: 8.46	0.05	34.1658	0.25	106.8784	0.17	3.9	0.91
9-22-77	(47)	5:20:27.38	0.11	34.3506	0.37	106.8960	0.24	7.4	2.39
9-22-77	(46)	19:19:16.39	0.09	34.3329	0.23	106.8897	0.21	11.5	1.13

the 83 events observed to have significant S wave frequency attenuation, 42 were unable to be used because of either (1) a poor hypocenter location or, (2) insufficient stations in the array to produce a reliable location (two stations or less). Also included in Table 3 are the locations of five microearthquakes in which no attenuation of either the P or S waves occurs at any of the recording stations (dates marked by an asterisk).

THEORETICAL DISCUSSION

Suggested causes for attenuation of the S wave in microearthquakes are (1) variation of source parameters, (2) spectra variation with change in azimuth around the focus, (3) normal loss of the higher frequency components of the spectra because of the distance traversed, (4) station effects, and (5) travel through an anomalous volume of the crust.

It is well known that earthquake spectra are a function of certain source parameters. Among the most important of these are fault size (dislocation area) and velocity and acceleration of rupture. In addition, magnitude and stress drop can be calculated from an analysis of earthquake spectra. For a complete discussion of these parameters see Brune (1970), Knopoff and Mouton (1975), and Randall (1973). For the same source model, however, the spectra for the P and S waves should be identical at the time rupture occurs. Thus if an abnormally low dominant frequency is observed in the S wave it should also be present in the P wave if source parameters are the only cause. Events in which P and S have similar frequency content are shown in the photographs of Plate 3. The effect of source parameters was eliminated in the data collection process by choosing only those events in which the frequency content of the S wave was substantially lower than the P wave.

SEPTEMBER 3, 1976 SC
13:25 UST

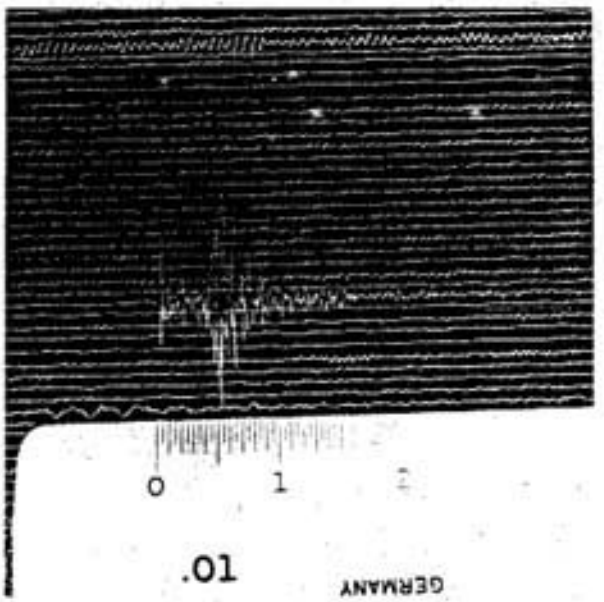

AUGUST 24, 1977 CM
11:22 UST

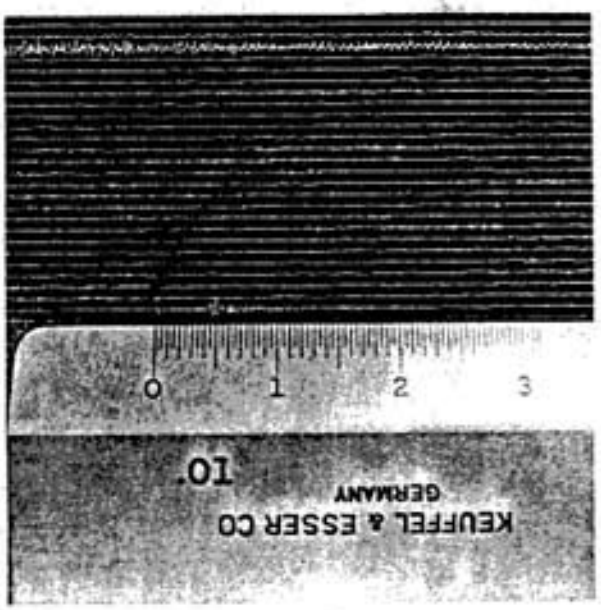

APRIL 15, 1976 SC
18:28 UST

APRIL 13, 1976 IC
9:45 UST

Plate 3. Examples of events in which the P and S waves have similar frequency content.

Variation of the spectra with change in azimuth around the focus is the second possibility. Due to the unequal distribution of energy propagated by the P and S radiation lobes (double-couple point source model) there could conceivably be some variation in the S wave spectra which would not necessarily be duplicated by the frequency content of the P wave. Douglas, Ryall and Williams (1971) performed a study on the variation of spectra with azimuth for microearthquakes in central Nevada. They averaged groups of spectra to eliminate peculiarities in individual records and considered events at approximately the same hypocentral distance. For the lengths and amplitudes of the seismic signals analyzed they concluded that the S wave contributed most significantly to the Fourier amplitude spectrum. They found, for six separate event groups, representing an azimuth range of approximately 140°, that there was no systematic variation of the spectra.

The third consideration is the normal loss of high frequency observed for raypaths traversing long distances through geologically complex volumes of crust. It is well documented in the literature (Sanford and Holmes, 1962, Douglas, Ryall, and Williams, 1971) that such losses occur and that the S wave, due to its transverse mode of propagation, is more susceptible to loss of the higher frequency spectral components than the P wave. However, from observations of the wave forms of microearthquakes arriving at stations from great (>30 km) distances it is quite apparent that the S wave suffers little of the unusual frequency attenuation of the type present in the data used in this study. A list of events of this type is presented in Table 4. In addition, an average dominant frequency was obtained for unattenuated microearthquakes, as they appear at stations FH, CC, WT and SC, from a zero-crossing counting

Table 4. Events with Unattenuated Arrivals at Distant (>30 km) Stations.

Event Date	Origin Time	Approximate Hypocentral Distance (km)	Recording Station
9-19-75	8:42:57.19	38.7	MG
		36.1	HC
11-5-75	14:35: 4.24	41.2	MY
6-3-77	20:45: 2.77	30.6	LAD
		33.2	CM
7-14-77	10:00:32.48	34.5	GM
		37.3	LAD
7-19-77	6:16:54.87	33.5	GM
8-18-77	9:30:13.35	33.5	GM
9-1-77	18:20: 2.29	45.4	GM
9-20-77	1:20: 8.62	46.4	RI
		49.9	TD
9-21-77	6:19: 8.46	41.8	RI
9-22-77	5:20:27.38	31.3	RI
		32.2	TD
9-22-77	19:19:16.39	39.7	GM
		33.0	RI

analysis of a random selection of events recorded on the digital DR-100 units. This data is presented in Table 5. These results were considered typical of microearthquake activity in the Socorro area. The events listed in Table 5 were considered 'normal' for the area in that they possess the frequency requirement for whiteout on an MEQ-800 record. The dominant frequency found for the P wave was 19.7 Hz (s.d. 1.5 Hz), the S wave was 12.3 Hz (s.d. 0.3 Hz). Considering the wide range of hypocentral distances and amplitudes included in this analysis, the standard deviations for the dominant frequencies are quite small. This also indicates that frequency attenuation in the S wave is not strongly dependent on the distance, alone, traversed in the crust of the Socorro area.

The fourth possibility is that anomalous S wave frequency attenuation occurs in the near surface geological column directly beneath the stations. Whenever possible, the stations were located on solid rock off the deep alluvial fill present in much of the La Jencia and Socorro basins, so that this effect should have been minimized. However, the station corrections which appear in Table 2 indicate that there may be substantial differences in geology beneath the stations. To determine if this was a factor influencing the spectra of the S wave, seismograms showing unattenuated S waves, for a varied azimuth range, were found for each station showing anomalous S wave attenuation, except BG. The special case for the station BG will be discussed under conclusions. These unattenuated raypaths often travelled through the same station material the attenuated raypaths traversed. Stations for which this occurred are CM, SC, FM, DM, CC, GM, and NG. A list of the events which were sources for these raypaths, and the stations at which they were observed, unattenuated, is

Table 5. Data for Determination of Unattenuated Dominant Frequencies.

Event Date	Approximate Origin Time	Recording Station	Dominant P Wave Frequency	Dominant S Wave Frequency
5-30-77	6:55	SC	19.56	12.11
5-30-77	7:01	CC	17.77	12.42
5-30-77	7:25	SC	23.10	12.11
5-31-77	5:48	SC	18.73	11.83
6-2-77	6:50	SC	18.39	11.50
6-3-77	3:49	SC	19.60	12.49
8-9-77	9:50	WT	17.46	10.97
8-11-77	9:54	CC	22.32	12.70
8-17-77	12:08	CC	17.42	12.29
8-17-77	14:14	CC	19.53	11.68
8-18-77	8:11	CC	19.11	12.16
9-1-77	21:59	WT	18.06	12.47
9-22-77	5:20	WT	19.55	11.95
10-18-77	8:16	SC	20.71	13.48
11-15-77	19:02	FM	23.99	14.13

given in Table 6. Assuming, more generally, that the geological section beneath each station is approximately uniform azimuthally near (~0.50 km) the station, then the highest dominant frequency S wave observed passing through that section should be close to the value observed for every incoming travel path. This assumes the ray has not already passed through an anomalously attenuating volume. If this is a valid approximation, then the observation of just a few unattenuated raypaths at a station is sufficient to justify minimizing station effects as the cause of the anomalous S wave attenuation. Furthermore, the criterion that the P wave be high frequency when attenuation is observed in the S wave is also beneficial in eliminating station effects, as one would expect some attenuation of the P wave to occur for such great attenuation in the S wave. This would be particularly true for attenuation due to the static frictional dissipation encountered in granular media. The manner in which the data was collected precludes this possibility. Thus, station effects alone do not seem to be able to account entirely for the frequency attenuation observed in the S wave.

The fifth possibility is an anomalous region in the crust through which the raypath traverses, which causes the observed frequency attenuation in the S phase. Walsh (1969) has theoretically analyzed a model of partially melted rock. The model consists of the melt occurring as thin films along grain boundaries. The melt thus makes up a very small fraction of the total volume of the rock. Walsh derived expressions for the complex bulk modulus and rigidity. He found that rigidity and attenuation in pure shear depend on the number of sites at which melting has occurred rather than the total concentration of the melt. Response in pure dilatation, though, is a function of concentration alone. The

Table 6. Unattenuated Raypaths for Determination of Station Effects.

Event Date	Approximate Origin Time	Recording Station(s)
5-22-75	11:36	CC, CM
7-30-75	21:44	CM, CC
8-8-75	10:53	FM
8-19-75	8:11	SC, CC
8-19-75	10:00	CM, SC
8-20-75	12:20	CM, SC
8-25-75	19:37	CC
9-19-75	8:42	GM
11-7-75	13:52	CC
1-23-76	2:53	SC
4-20-76	8:32	DM
4-23-76	5:57	DM
8-10-76	4:38	NG
10-6-76	15:12	DM
2-9-77	10:59	NG
2-10-77	7:33	CC
4-15-77	6:35	GM
4-27-77	12:23	CC
6-2-77	6:50	GM
6-3-77	20:45	CM
6-3-77	23:01	CM
7-14-77	10:00	GM
7-19-77	6:16	GM
8-17-77	2:20	GM
8-24-77	11:22	NG
9-1-77	18:20	GM
9-1-77	21:58	NG

result is that attenuation in pure dilatation is low and bulk modulus is approximately equal to the value obtained for unmelted material. Thus for a partial melt of very low total concentration one would theoretically expect a great effect on the S wave spectra but little or no change in the P wave spectra.

Due to the difficulty of reproducing the conditions of a partial melt in the laboratory direct experimental verification of the results outlined above is lacking. However, Spetzler and Anderson (1968) were able to study the effects of another type of partial melt on attenuation in longitudinal and shear waves. They investigated the attenuating properties of a simple binary system of $NaCl \cdot H_2O$. Research was conducted in the range from a complete solid at low temperature to a 17 percent melt at higher temperatures. As a solid the system was a mixture of H_2O (ice) and $NaCl \cdot 2H_2O$. At higher temperatures the system was a mixture of ice and NaCl brine. In the completely solid regime, seismic velocities and Q (quality factor) changed slowly with increasing temperature. At the onset of melting, though, there was a marked decrease in both seismic velocities and Q. The authors concluded that a small fraction of liquid has a large effect on seismic velocities and Q, and that the shear wave was considerably more affected than the longitudinal wave. In addition, the most dramatic and pronounced effects occurred at the onset of melting rather than in melts with higher percentages of fluid. These conclusions, obtained experimentally, are remarkably similar to the theoretical results obtained by Walsh (1969).

A study more closely related to the situation believed to exist in the Socorro area is the work done by Matumoto (1971) in the vicinity of Mount Katmai, Alaska. He observed the absence, or almost complete

absence, of the S wave for certain microearthquakes recorded in that region. Shuleski (1976) observed a similar effect in the Socorro area. The S wave screening observed by both Matumoto and Shuleski was explained by the passage of the raypath in which screening was observed through a magma body or chamber. Matumoto also observed some attenuation of the higher frequencies in the P wave spectra for the cases in which the S wave was completely absent. This also appears to be the case, to a lesser degree, for some of the events used in this study. In some cases, parts of the P wave would not always completely fulfill the whiteout criterion discussed above. This indicates that, for the more severe cases of S wave attenuation, the P wave is also affected to a lesser extent. The effect was never so great, however, that an accurate measurement of the dominant frequency of the P wave could be measured by the zero-crossing counting technique on the MEQ-800 records.

From the discussion above it is apparent that a partial melt of very low liquid concentration has an abrupt and significant effect on shear waves. It is possible that the magnitude of the attenuation observed in the shear waves of microearthquakes in the Socorro area is not severe enough to warrant postulation of a partial melt. Instead, the anomalous regions may be volumes of very hot rock at a temperature well below the liquidus. This could result in a less severe absorption of the seismic energy of the shear wave than would be the case if the S wave traversed a volume of partial melt. Evidence for this possibility is indicated in a paper by Solomon (1972). The relevant results are presented in Figure 5. The increase of Q, first seen in the samples for moderate temperatures, is probably the result of a loss of moisture. However, at higher temperatures (approximately 450°C to 500°C) the trend abruptly reverses

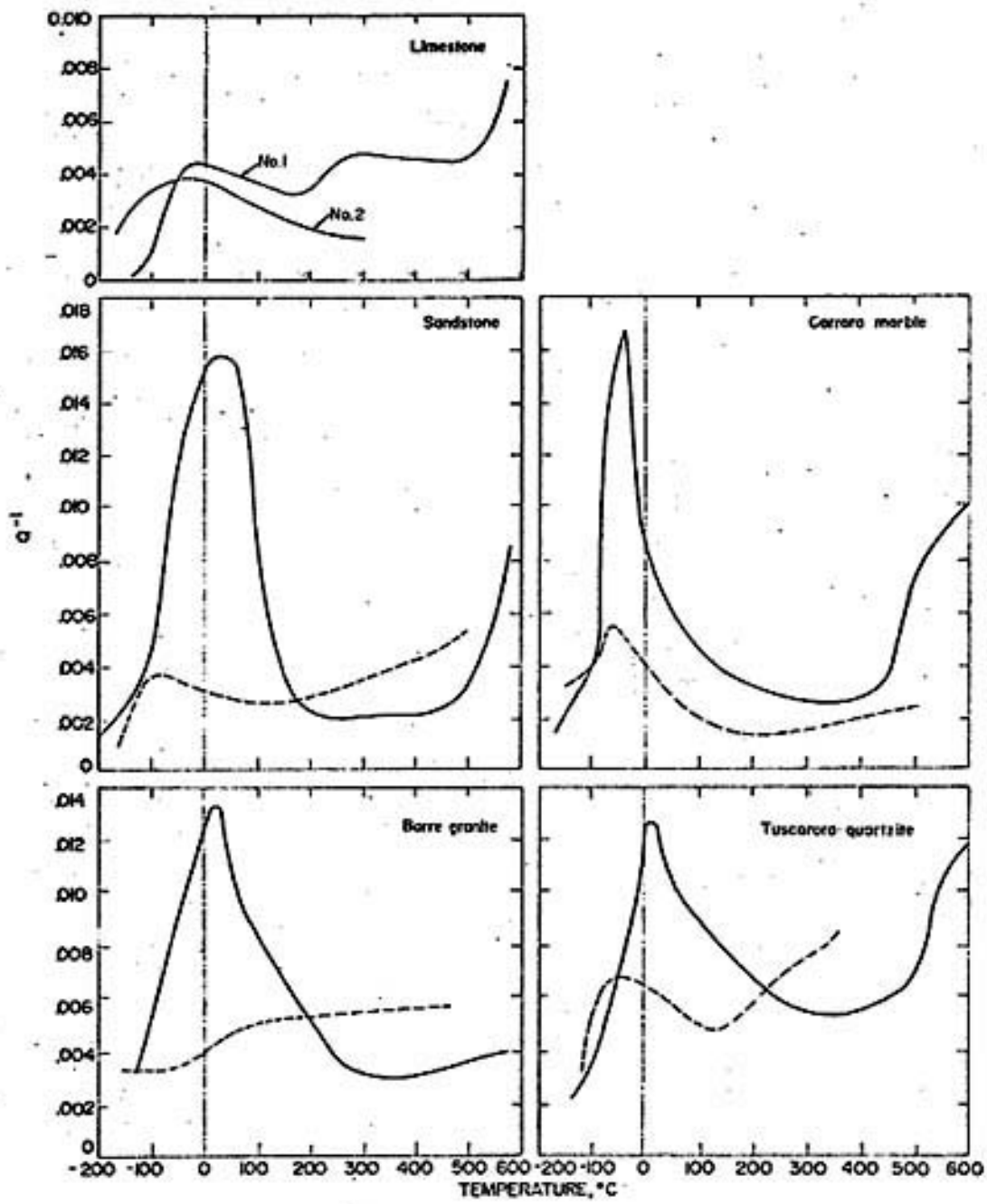

Figure 5. Q as a function of temperature, at surface pressure, for various rock types (from Solomon, 1972).

and a significant decrease in Q occurs. The effect is observed up to the last temperature plotted (600°C) for all samples. The experiment was conducted at surface pressure. Extrapolation of these results to higher temperatures could lead to a value for Q which explains the absorption of seismic shear wave energy in the Socorro crust.

From the results obtained in the studies discussed above it appears that a low value of Q for shear waves propagating in the vicinity of a partial, or near partial, melt leads to a selective loss of the higher frequencies in the amplitude spectra. This yields a decrease in the dominant frequencies observed on the seismograms as measured by the zero-crossing counting technique. From the magnitude of the decrease observed in the S wave, a crustal anomaly that could be postulated is a volume of heated rock whose temperature is somewhere below the liquidus.

INTERPRETATION

Primarily, the interpretation of the data consisted of mapping the raypaths along which attenuation of high frequencies occurred in the S phase. The volumes of crust defined by the intersection of these raypaths were then identified as possible regions of heated rock. The additional stipulation that these regions be free of hypocenters was also considered in their final placement. The high temperatures in a volume of heated rock would preclude the buildup of the elastic strain energy required for microearthquakes to occur. The high temperatures are thus assumed to promote stable sliding rather than stick-slip movements in the volumes of heated rock (Brace and Byerlee, 1966).

Also considered in the analysis were those raypaths along which no frequency attenuation in either the P or S waves was observed. Theoretically, these raypaths should not cross the regions of heated rock and

were thus used to eliminate anomalous areas which appeared at more than one location along a raypath.

A three-dimensional scale (0.392 in. = 1 km) model was constructed to aid in the spatial placement of the volumes. The general layout of the model may be seen in the photographs of Plate 4. The model consists of a styrofoam base (2 in. x 2 ft. x 2 ft.) with four plexiglass rods mounted perpendicular to the base at each of its four corners. Supported horizontally on these rods is a plexiglass sheet (0.25 in. x 2 ft. x 2 ft.) with its top surface parallel to the styrofoam base, 7.84 in. (20 km) above the base. The top surface of the plexiglass sheet is a map representing an area which extends approximately 33.7 km W, 27.8 km E, 16.5 km S, and 44.8 km N of Socorro (total area: 3748 km^2). Marked on this map are the major towns, seismic stations used (two and three letter designations), and the epicenters (numbered). Below each epicenter is a black polystyrene bead (average diameter: ~0.25 in.) mounted on a 2 mm diameter glass rod supported in the styrofoam. The distance from the top of each bead to the top surface of the plexiglass sheet is the model depth for the respective hypocenter. The size of the beads gives a rough idea of the error bars associated with a typical hypocenter location. See Table 3 for the actual error bars associated with a particular hypocenter. Attached to the tops of the beads are threads representing seismic raypaths. The threads are of three different colors, representing three separate groups into which the data was subdivided (1) blue, raypaths where both P and S waves are unattenuated, (2) yellow, raypaths where the P wave is unattenuated but the S wave is ($8\ Hz \leq \nu_s < 12\ Hz$), and (3) red, same as (2) but the range for dominant S wave frequency is $\nu_s < 8Hz$. The threads are attached to the stations at which raypaths

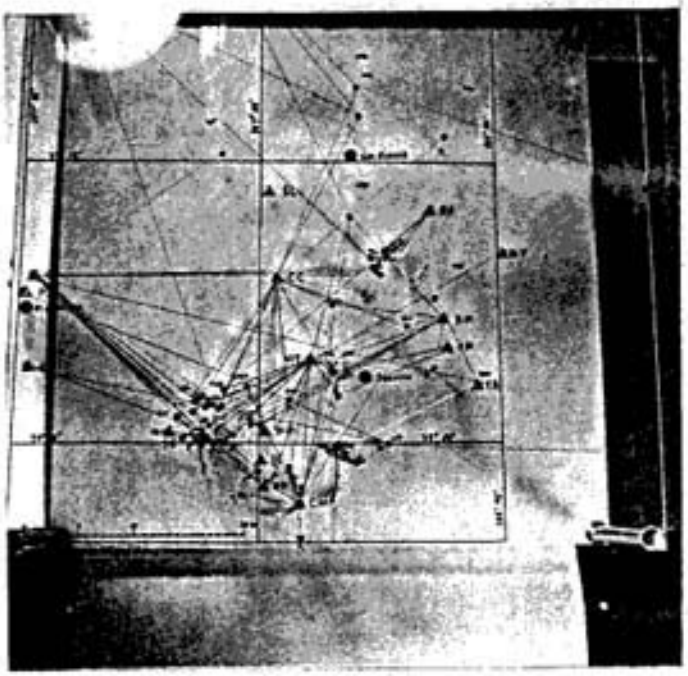

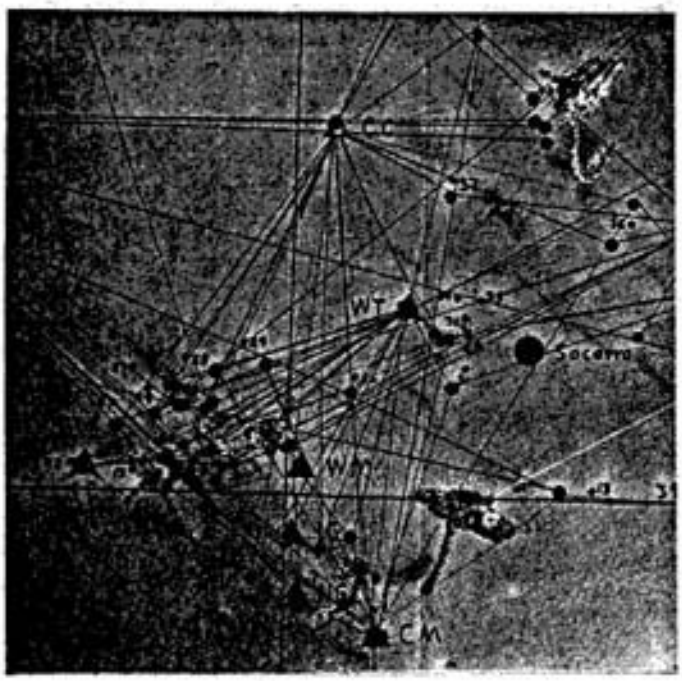

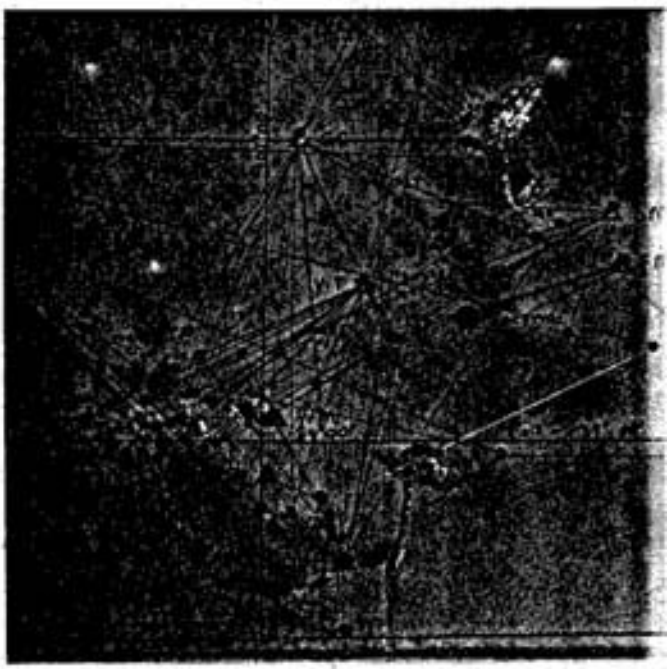

Plate 4. Top views of the three-dimensional model.

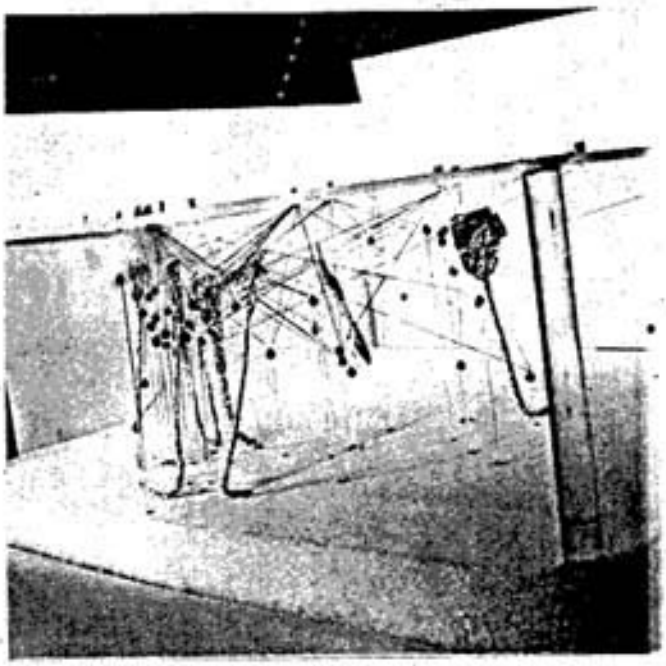

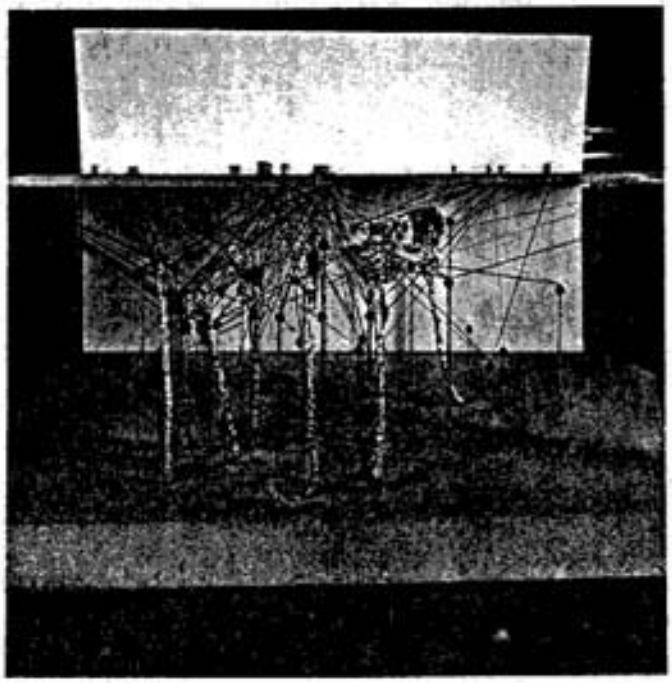

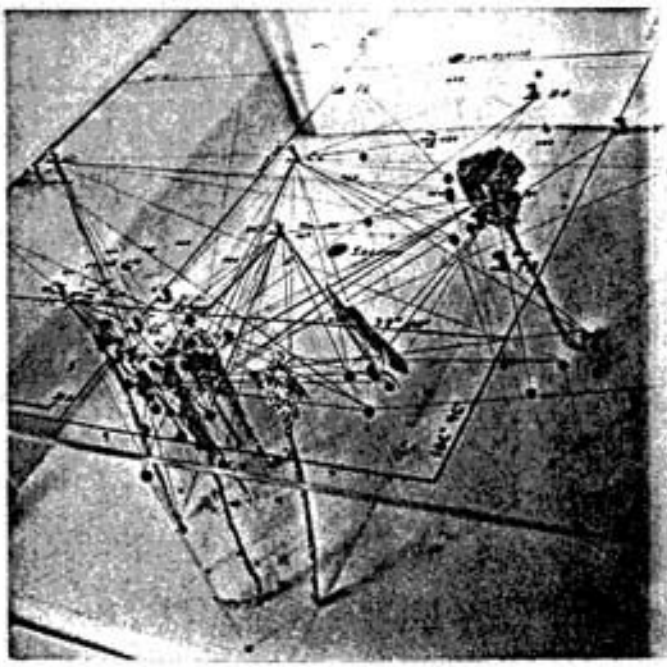

Plate 4. (Continued) Side views of the three-dimensional model.

exhibiting criteria (1), (2), or (3) were observed. The data was subdivided into groups (2) and (3) to attempt to define portions of the anomalous volumes which were of higher temperature than others. It was thought this would also indicate the complexity of the shapes of the attenuating volumes.

The primary advantages of using the three-dimensional model rather than a simple two-dimensional surface projection for interpretation are (1) regions can be defined which appear to overlap an area of epicenters at the surface, (2) minimum depth to the region is easily defined, and (3) interpretation of raypaths of type (1), which pass close to raypaths of type (2) and (3), is easier.

The main objective of interpretation using the model was to explain as many of the attenuated raypaths as possible with a minimum number of volumes. Pieces of aluminum foil were used to experiment with placement of the volumes as they were readily able to be moved about and introduced into the spaces between the thread. It became immediately obvious during placement that the attenuating volumes are not of simple shape but highly irregular. Raypaths of type (2) and (3) crisscross the zones with no obvious systematic spatial variation. Often, type (1) raypaths cross near a clustering of type (2) and (3) raypaths, further indicating that not only are the volumes complex in shape, but the boundary between the attenuating volume and country rock is probably quite sharp. Some of these features may be seen in the photographs of Plate 4. The final approximate locations of the attenuating volumes are represented by the placement of the eight pieces of aluminum foil. The long stems attached to the upper, broader portions of foil have no physical meaning, but only serve to support the upper part of the foil in the correct position.

Eight separate volumes have been proposed to account for all but three of the attenuated raypaths. Two of these raypaths cross areas in which there is otherwise very little data. They are common to a region approximately 7 km southeast of the station SL, at a depth near 6 km, but there is not enough data to postulate an anomalous volume. The third raypath (from hypocenter (37) to DM) also crosses a region lacking in data. No attempt has been made to explain its presence. It is interesting to note, though, that the error bar for the depth in the location of event (37) is unusually large (3.19 km), indicating that whatever is causing the absorption may exist at a greater depth than appears to be the case from the depth listed in Table 3 for the hypocenter.

The locations (longitude, latitude, and depth) of the eight proposed volumes, as well as the number, type, and hypocenter origin of the raypaths used in the interpretation of each volume, are listed in Table 7. The epicenters of the events listed in Table 7 are plotted in Figure 6. Unattenuated raypaths used in the interpretation are listed as well. Figures 7 and 8 show maps of the locations of the attenuating volumes relative to the epicenters of the study, the surface projections of the attenuated raypaths, and the general physiographic features of the Socorro area. The latitudes, longitudes, and depths given in Table 7 roughly locate the shallowest points of the tops of the anomalous zones. In Figure 7, type (2) raypaths indicate potentially lower temperature rock than type (3) raypaths.

CONCLUSIONS

An alternate interpretation to the heated rock theory to explain the absorption discussed above is suggested by the work of Wallace (1978). He relates microearthquake swarm activity to magmatic intrusion in the

Table 7. Locations of Proposed Attenuating Crustal Volumes and the Defining Raypaths.

Volume*	Longitude	Latitude	Depth (km)	Raypaths Used for Volume Location		
				Hypocenter Origin**	Type	Recording Station
1	106.8591	34.1734	2.9	47	2	FM
				46	2	FM
				41	2	BG
				40	2	BG
				42	3	BG
				39	2	BG
				43	3	DM
2	106.9194	34.9573	3.2	34	2	FM
				32	3	FM
				33	2	FM
				20	3	DM
3	106.9096	33.9988	3.4	31	3	CM
				38	3	CM
				13	3	CM
				30	2	NG
				13	1	HC
				13	1	MG
4	106.9610	33.9686	3.6	7	3	CM
				4	3	CM
				6	3	CM
				34	1	CM

Table 7. Continued

Volume*	Longitude	Latitude	Depth (km)	Raypaths Used for Volume Location		
				Hypocenter Origin**	Type	Recording Station
4	106.9610	33.9686	3.6	33	1	CM
				26	2	CM
				5	1	CM
				43	1	CM
5	107.0132	34.0310	4.6	9	2	DM
				14	2	DM
				28	3	CM
				29	3	CM
				16	3	DM
				17	3	DM
				16	1	WT
				17	1	WT
				20	1	SC
				13	1	HC
6	107.0483	34.0314	7.1	21	1	CC
				21	1	WT
				18	2	CC
				10	2	CC
				23	2	CM

Table 7. Continued

Volume*	Longitude	Latitude	Depth (km)	Raypaths Used for Volume Location		
				Hypocenter Origin**	Type	Recording Station
7	107.0651	34.0496	8.7	25	2	GM
				27	2	CC
				8	3	BG
				27	1	WT
8	107.0752	34.0156	4.1	22	3	CM
				11	2	SC
				3	1	SC
				15	3	SC
				21	2	SC
				9	1	GM
				48	3	CM
				24	2	SC
				19	1	HC
				19	2	SC
				16	1	SC

* See Figure 7 for crustal volume coding
** See Figure 6 for hypocenter coding

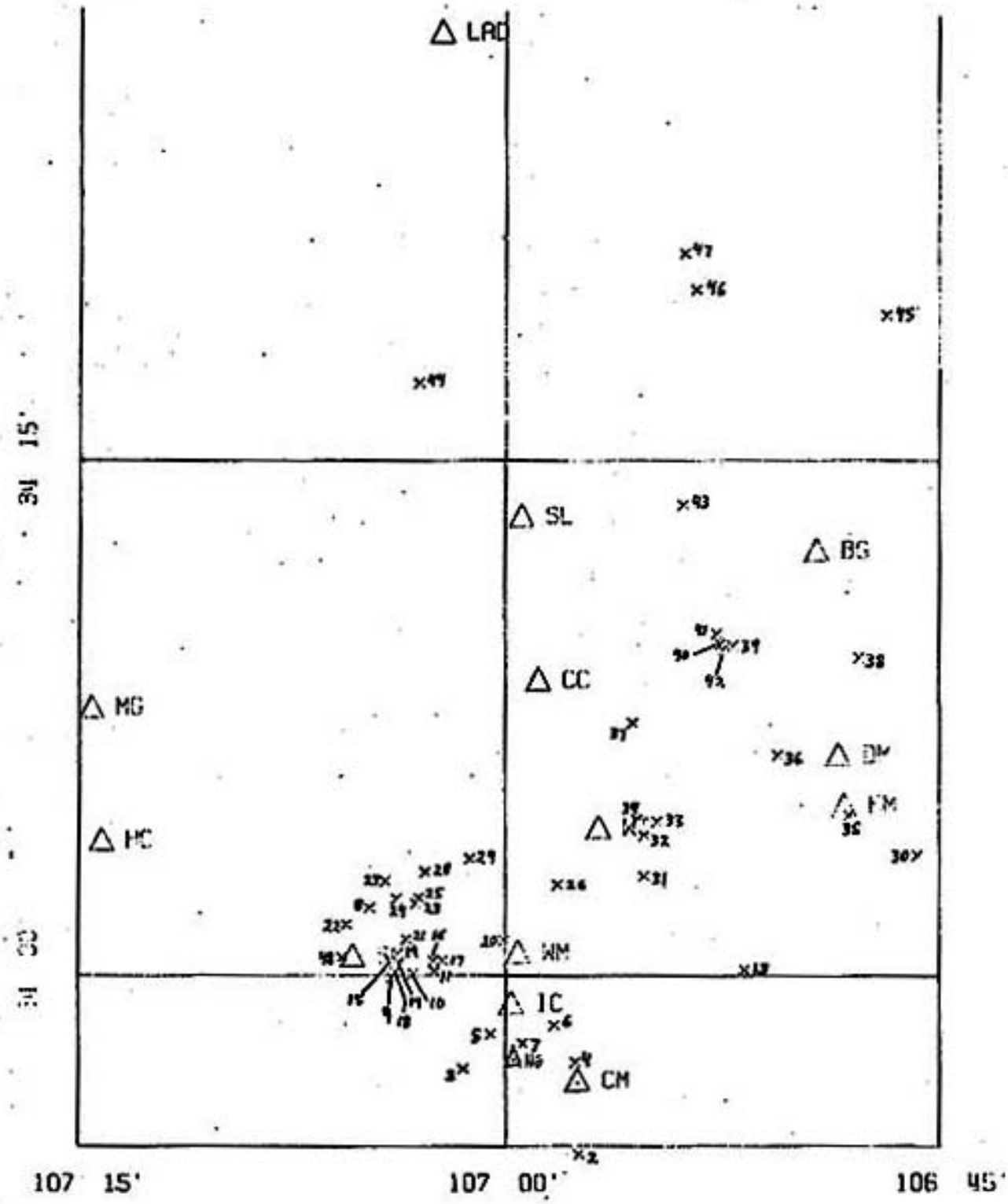

Figure 6. Hypocenter coding used in Tables 7, 8, and in the text.

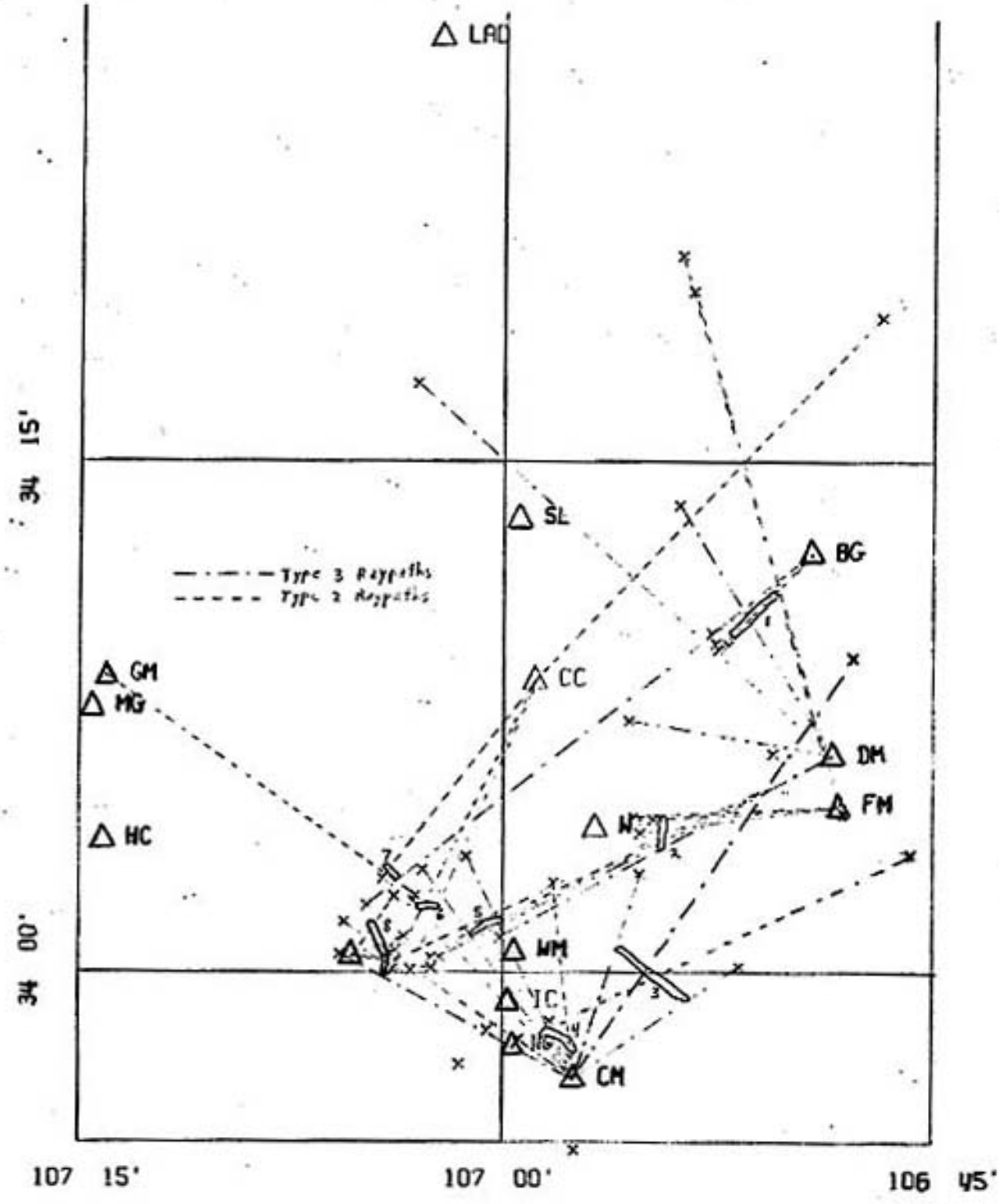

Figure 7. The positions of the eight proposed attenuating volumes of crustal rock relative to the attenuated raypaths, and the epicenters.

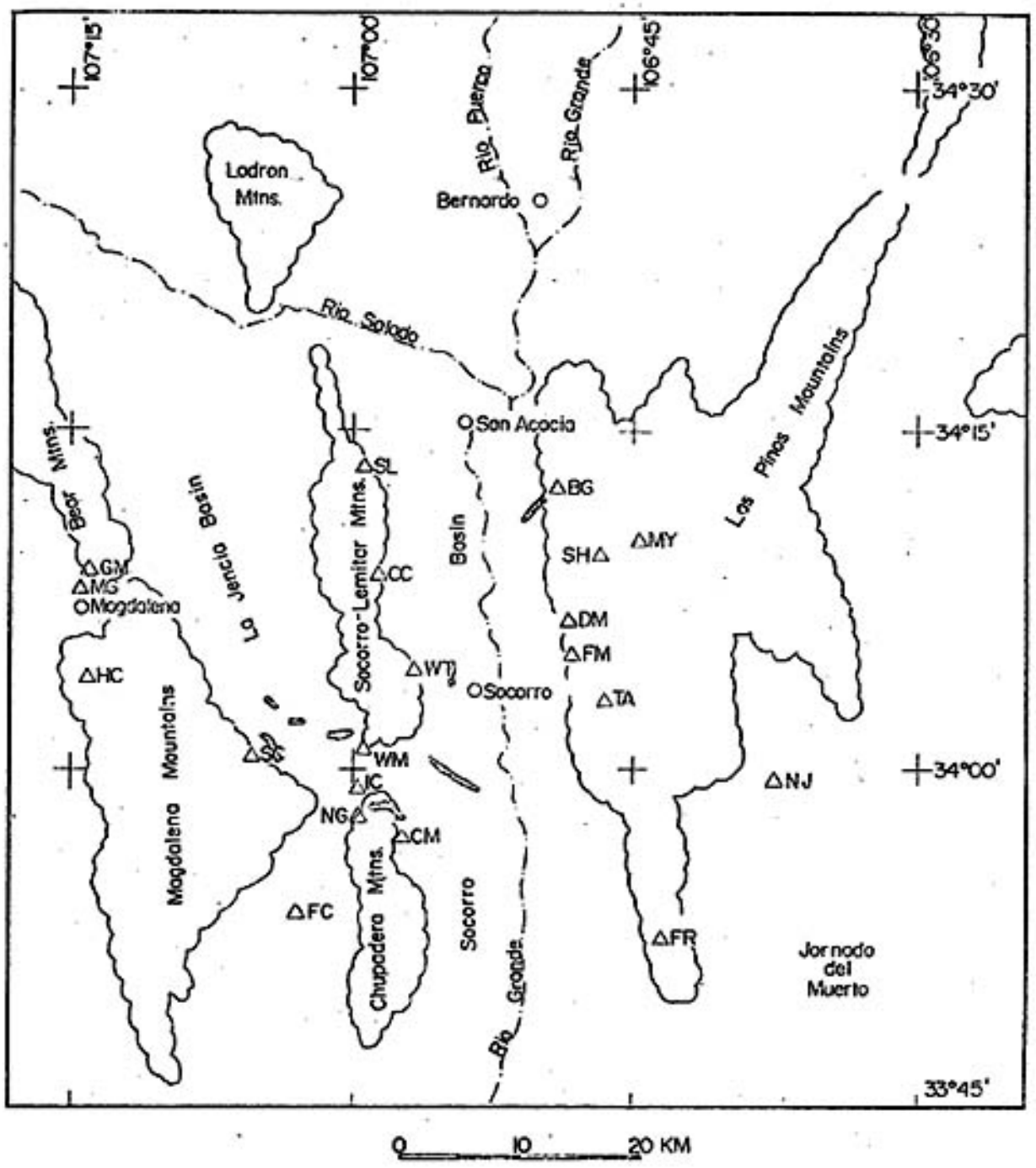

Figure 8. The positions of the eight proposed attenuating volumes of crustal rock relative to the physiographic features of the Socorro area.

Socorro area. He concludes that the model most likely to explain seismic swarm activity and an associated high b-value (1.38) starts with microfracturing of the crust due to magma injection, possibly to dilatancy, then strain release occurring at some later time due to the circulation of hydrothermal solutions migrating to the zone of microfracturing. If the volume of microfractures makes up a significant percentage of the total volume of the rock, and the fractures are fluid-filled, then it is possible that this could cause the type of absorption observed in the S waves in this study. These volumes would still approximately define the possible position for partial melts, as the microfracture zones would probably occur above, and adjacent to, a partial melt. They would then appear, as would the volumes in the heated rock theory, at a depth shallower than the partial melt.

Wallace further concludes that microearthquake swarms, for the most part, will be confined to crustal regions adjacent to shallow magma bodies and that the high b-value indicated above reflects structural heterogeneity. Figure 9 is a map locating the swarms used by Wallace relative to the surface projections of the eight proposed attenuating volumes. In many instances, there is good correlation between the swarms and attenuating volumes in that the swarm activity often appears adjacent to the anomalous volumes. The depth of the swarms is generally deeper than the anomalous volumes. The diffuse nature of the swarm activity in the southern La Jencia basin indicates a great structural heterogeneity which may accompany the presence of the large number of attenuating volumes proposed in that area. Only one swarm appears to be associated with the volume appearing southwest of the station BG. This could be the result of a data set which is less inclusive than the one used in this study.

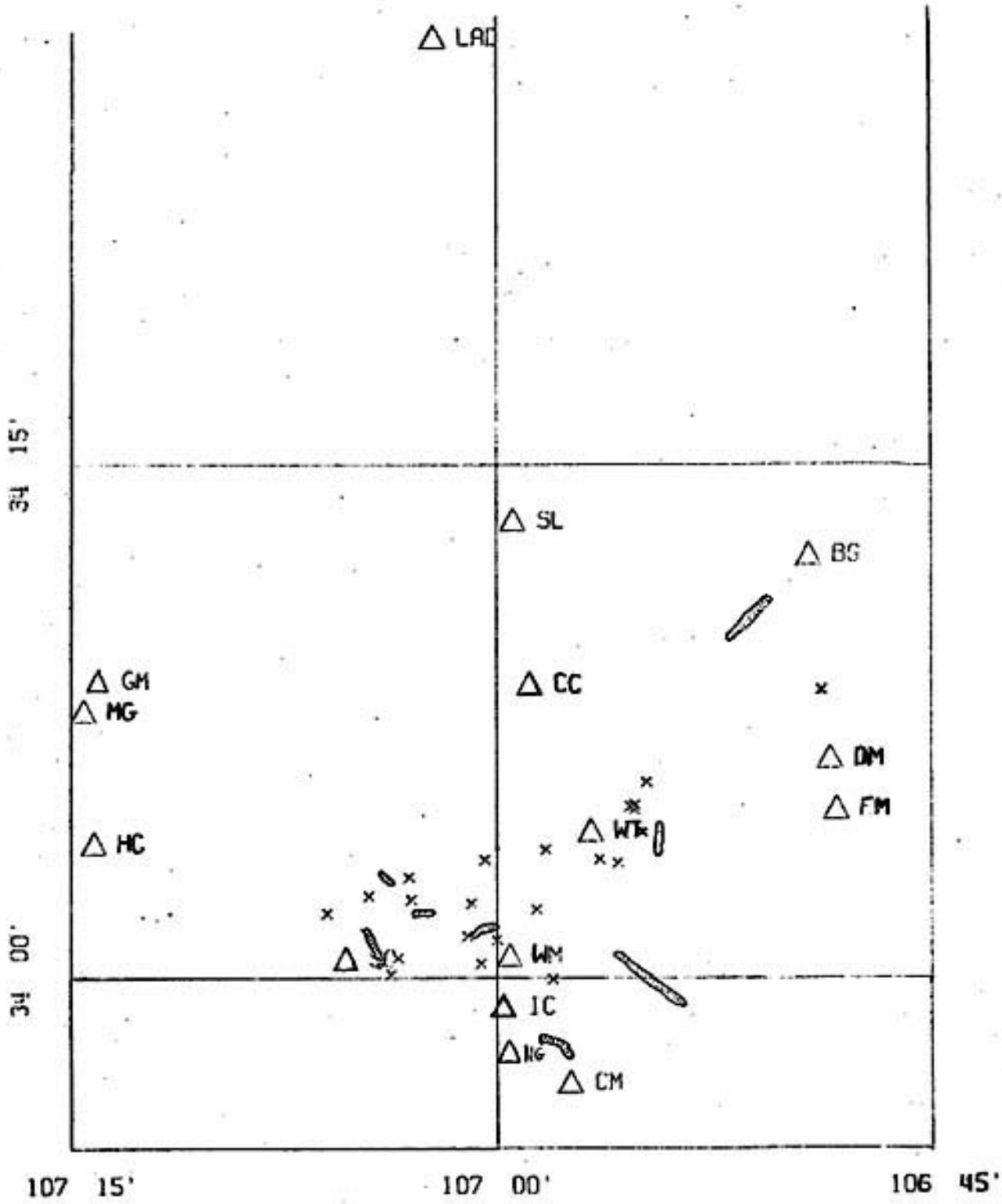

Figure 9. The positions of the eight proposed crustal volumes relative to the microearthquake swarms located by Wallace (1978).

Wallace used data from June, 1975 to June, 1977. The seismic arrays were moved farther north soon afterward, enhancing the collection of data in the area around the station BG.

Of the three theories presented to explain the anomalous absorption occurring in the S wave, (1) partial melting, (2) heated rock, and (3) fluid-filled microfractures, the second appears to be the most probable. The observed absorption may not be great enough for a partial melt to be the cause, and the percentage volume of fluid-filled microfractures may not be great enough for this to be a cause. As is pointed out in the Appendix, absorption of energy in ordinary rock matrix pore space, filled with fluid, is insignificant for seismic frequencies (<100 Hz). If the amount of fluid present does not make up a significant portion of the rock volume, it will have little affect on absorption of seismic shear wave energy.

One of the primary assumptions made in the interpretation above is that dominant frequency is directly proportional to the quality factor, Q. Thus a decrease in dominant frequency has been associated with a lower Q value and increased absorption. A relationship between Q and dominant frequency, ν, has been proposed and justified in the Appendix. The relevant relation is,

$$Q_\alpha/Q_\beta = \nu_\alpha/\nu_\beta \quad , \tag{2}$$

where the subscripts α and β refer to P and S waves, respectively. The value of this ratio, using the unattenuated dominant frequencies determined from the data in Table 5, is 1.60. An increase in this ratio should indicate that Q_β is decreasing relative to Q_α and thus the absorption of the shear wave is increasing. Table 8 lists all attenuated raypaths with their associated Q_α/Q_β ratios. In the calculation of the ratio,

Table 8. Attenuated Raypaths and Associated Q_α/Q_β Ratios

Raypath		Q_α/Q_β
Hypocenter Origin*	Recording Station	
34	FM	1.71
33	FM	2.05
31	CM	3.85
26	CM	2.11
32	FM	3.24
13	CM	2.55
38	CM	3.22
6	CM	2.96
20	DM	4.02
37	DM	3.96
21	SC	2.37
14	DM	1.89
43	DM	2.66
39	BG	2.43
48	CM	3.17
4	CM	2.55
28	CM	4.22
7	CM	3.08
29	CM	2.59
27	CC	1.80
8	BG	2.91
19	SC	1.70
24	SC	2.00
18	CC	1.82
9	DM	1.94
42	BG	2.51
15	SC	1.75
46	FM	2.25
41	BG	2.27
25	GM	2.33

Table 8. Continued

Raypath		Q_α/Q_β
Hypocenter Origin*	Recording Station	
22	CM	3.09
45	CC	2.22
40	BG	2.40
44	DM	3.36
23	CM	2.40
47	FM	2.45
10	CC	1.90
17	DM	2.89
16	DM	2.71
11	SC	1.97
30	NG	2.31

*See Figure 6 for hypocenter coding

the dominant frequency of the P wave was assumed constant, within one standard deviation, of the value 19.7 Hz. This was considered a good approximation for P waves fulfilling the whiteout criterion. The larger the ratio, the greater is the absorption of S wave relative to P wave energy and, presumably, the hotter is the material the associated raypath has traversed. This does not alter the results obtained above but serves to relate those results to a more appropriate measure of absorption, Q, appearing in the literature reviewed in the theoretical discussion section.

By averaging the raypath values of Q_α/Q_β which define a particular volume, it is possible to assign a mean relative absorption factor to that volume. Table 9 lists the volumes determined in the interpretation section and their respective mean Q_α/Q_β ratios. These values are possibly low as an average for the entire volume, because the raypaths used to locate the attenuating volumes probably define their boundaries. S waves traversing the center, hotter portions of the volumes are likely to be completely screened. This argument primarily applies to the partial melt, or perhaps heated rock theory, to explain the anomalous volumes. If the absorption is due to fluid-filled microfractures, the Q_α/Q_β ratios will be closer to the true average for the entire volume as there should be little change in the absorbing characteristics of the center of the region relative to its boundaries. S wave energy should thus be able to propagate through all parts of the volume. Whatever the cause, the values listed in Table 9 are directly proportional to the amount of absorption occurring within the respective anomalous volume.

It should be emphasized that a good deal of potentially valuable data had to be eliminated due to poor hypocenter locations. It should

Table 9. Proposed Attenuating Volumes and Associated Q_α/Q_β Ratios.

Volume	Mean Q_α/Q_β	Standard Deviation
1	2.42	0.14
2	2.76	1.07
3	2.98	0.69
4	2.68	0.44
5	2.71	0.85
6	2.04	0.31
7	2.35	0.56
8	2.29	0.61

not be assumed, therefore, that all possible anomalous crustal volumes have been located, nor that the ones that have been located are accurate. The volumes which are probably related to shallow magmatic intrusion, and which are most accurately located, are (1) the region to the east of WT (depth: -3.2 km), (2) the region to the northeast of SC (depth: -4.1 km), and (3) the region to the northwest of WM (depth: -4.6 km). The poorest established relation between a proposed anomalous volume and magmatic intrusion is for the region southwest of BG. Most of the raypaths which defined the volume were observed at BG, a station where the absorption effects of the local geology could not be accurately determined. For each of the attenuated raypaths, the P wave conformed to the whiteout criterion, but an S wave was never observed at BG which satisfactorily fulfilled the whiteout criterion. Control of station effects was thus not as complete as for the other stations. The spatial extent of intrusive activity near BG may be such that it is rare to observe unattenuated S waves from the areas of microearthquake activity located to date. It is for this reason, and the observation of additional raypaths traversing the volume which are seen attenuated at stations other than BG, that the volume has been included.

Future studies could reveal that many of the proposed attenuating volumes are related or connected to each other. To obtain a truly accurate and detailed model of the variation of Q within the crust a great deal more data is needed. Preferably, this data would be in digital form so that a detailed spectral analysis of each raypath could be made. This would allow the absolute determination of Q for both P and S waves for each raypath. The crust could be subdivided into cubes and the raypaths plotted within the subdivided volume. Each time a raypath crossed

a cube the cube would have that value of Q associated with it (see Figure 10). All Q values for each cube could be averaged and the standard deviation calculated. Those cubes with Q values possessing an acceptably low standard deviation would be assigned that Q value. Q could then be three dimensionally contoured, or anomalous volumes constructed from cubes with similar Q values. With a sufficient amount of data the entire analysis could be readily performed on a digital computer with a graphics terminal. The final output might be most revealing in the form of a lucid, three-dimensional plot in which all the cubes are shown marked in their centers with their respective mean Q values.

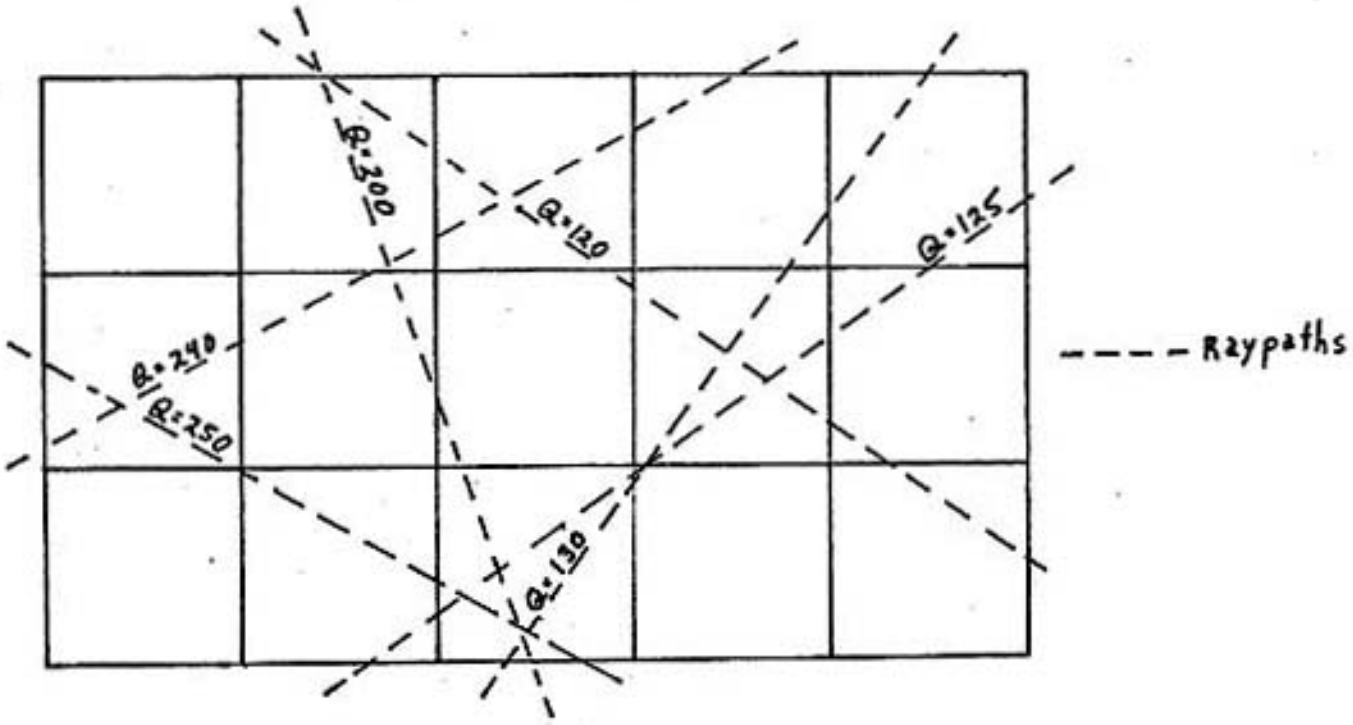

Figure 10. Top view of subdivided volume. The cubes take on the values of the raypaths crossing them.

ACKNOWLEDGMENTS

I would like to thank Dr. Allan R. Sanford for offering his assistance in all aspects of the research and writing of this paper. I also express appreciation to Eric Rinehart and Mark Frishman for their

photographic expertise; Roger Ward, for the use of his inversion program; Terry Wallace and John Fender, for their hypocenter locations, and Kent West for his efforts in data acquisition. Particular thanks is extended to my wife, Pam, for her patience and understanding.

REFERENCES CITED

Brace, W. F., and J. D. Byerlee, Stick slip as a Mechanism for Earthquakes, Science, 153, pp. 990-992, 1966.

Brune, J. N., Tectonic Stress and the Spectra of Seismic Shear Waves from Earthquakes, Jour. Geophys. Res., 75, pp. 4997-5009, 1970.

Chapin, C. E., and W. R. Seager, Evolution of the Rio Grande rift in the Socorro and Las Cruces areas, N. Mex. Geol. Soc. Field Conf. Guideb., 26, pp. 297-321, 1975.

Douglas, B. M., A. Ryall, and R. Williams, Spectral Characteristics of Central Nevada Microearthquakes, Bull. Seismol. Soc. Amer., 60, pp. 1547-1559, 1970.

Knopoff, L., and J. O. Mouton, Can One Determine Seismic Focal Parameters from the Far-Field Radiation?, Geophys. J. R. Astr. Soc., 42, pp. 591-606, 1975.

Kubota, A., and E. Berg, Evidence for Magma in the Katmaí Volcanic Range, Bull. Volc., 31, pp. 175-214, 1968.

Matumoto, T., Seismic Body Waves Observed in the Vicinity of Mt. Katmai, Alaska and Evidence for the Existence of Molten Chambers, Geol. Soc. Amer. Bull., 82, pp. 2905-2920, 1971.

Randall, M. J., The Spectral Theory of Seismic Sources, Bull. Seismol. Soc. Amer., 63, pp. 1133-1144, 1973.

Reiter, M. A., C. L. Edwards, H. Hartman, and C. Weidman, Terrestial Heat Flow along the Rio Grande Rift, New Mexico and Southern Colorado, Geol. Soc. Amer. Bull., 86, pp. 811-818, 1975.

Richter, C. F., Elementary Seismology, W. H. Freeman, San Francisco, Calif., 1958.

Rinehart, E. J., The Use of Microearthquakes to Map an Extensive Magma Body in the Socorro, New Mexico Area, M.S. Independent Study, Geoscience Dept., New Mexico Inst. Mining and Tech., 1976 (Geophysics Open-File Report No. 10, Geoscience Dept., NMIMT).

Sanford, A. R., and C. R. Holmes, Microearthquakes Near Socorro, New Mexico, Jour. Geophys. Res., 67, pp. 4449-4459, 1972.

Sanford, A. R., O. S. Alptekin, and T. R. Toppozada, Use of Reflection Phases on Microearthquake Seismograms to Map an Unusual Discontinuity Beneath the Rio Grande Rift, Bull. Seismol. Soc. Amer., 63, pp. 2021-2034, 1973.

Sanford, A. R., R. P. Mott, Jr., P. M. Shuleski, E. J. Rinehart, F. J. Caravella, and R. M. Ward, Microearthquake Investigations of Magma Bodies in the Vicinity of Socorro, New Mexico, Geol. Soc. Amer. Abstr. Programs, 8, pp. 1085-1086, 1976.

Sanford, A. R., R. P. Mott, Jr., P. J. Shuleski, E. J. Rinehart, F. J. Caravella, R. M. Ward, and T. C. Wallace, Geophysical Evidence for a Magma Body in the Crust in the Vicinity of Socorro, New Mexico, Amer. Geophys. Union, Geophys. Mono. 20, pp. 385-403, 1977.

Shuleski, P. J., Seismic Fault Motion and SV Wave Screening by Shallow Magma Bodies in the Vicinity of Socorro, New Mexico, M.S. Indep. Study, Geoscience Dept., New Mexico Inst. Mining and Tech., 1976. (Geophysics Open-file Report No. 8, Geoscience Dept., NMIMT).

Solomon, S. C., Seismic-Wave Attenuation and Partial Melting in the Upper Mantle of North America, Jour. Geophys. Res., 77, pp. 1483-1485, 1972.

Spetzler, H., and Anderson, D. L., The Effect of Temperature and Partial Melting on Velocity and Attenuation in a Simple Binary System, Jour.

Geophys. Res., 73, pp. 6051-6060, 1968.

Wallace, T. C., Microearthquake Swarm Activity in the Socorro, New Mexico Area, Directed Study, Geoscience Dept., New Mex. Inst. Mining and Techn., 1978.

Walsh, J. B., New Analysis of Attenuation in Partially Melted Rock, Jour. Geophys. Res., 74, pp. 4333-4337, 1969.

APPENDIX

LOSS MECHANISMS AND Q FOR COMPRESSIONAL AND SHEAR WAVES IN SHALLOW CRUSTAL MATERIALS

by

James A. Johnston

Term Paper, Geophysics 524, N.M.I.M.T.

May, 1978

Abstract

Five loss mechanisms have been reviewed as to their importance in absorption observed in shallow (<20 km) crustal materials for a frequency range of <100 Hz (1) solid friction, (2) viscous, (3) relative motion of pore fluid and rock matrix, (4) thermoelastic, and (5) nonlinear theory. Parameters (3) and (5) are insignificant, (1) dominates by far, while (2) and (4) are less dominant. The quality factor, Q, is found to be essentially independent of frequency ($Q = 213f^{-0.015}$, $10^{-3} < f < 10^{7}$, Attewell and Ramana, 1966). The relation $Q_\alpha/Q_\beta = \nu_\alpha/\nu_\beta$ (α,β refer to P and S waves, respectively; ν is dominant frequency) is proposed. Q_α/Q_β is then 1.60 for the Socorro area as calculated from microearthquake data. It is shown how Q_α/Q_β can be used as a valuable constraint in earth modelling.

Introduction

The primary purpose of this paper is to review some of the different

mechanisms used to explain seismic absorption in shallow (<20 km) crustal materials. A realistic earth mechanism will then be justified to explain the absorption observed in the laboratory and field. Some idea of the magnitude of Q for the crust will also be determined. In addition, an effort will be made to formulate, as quantitatively as possible, a relation between the relative amounts of attenuation of compressional and shear waves in the range of frequencies of interest in seismology and seismic prospecting (<100 Hz). Finally, these ideas will be extended to the Socorro area and an indication of the degree of absorption normally occurring, estimated, by noting the frequency content of natural seismic activity (microearthquakes).

Attenuation in seismic waves is due to a variety of sources. The factors involved include geometrical spreading, energy loss at a reflecting boundary, dispersion, scattering, diffraction, and absorption. The attenuation to be discussed in this paper is concerned only with the last of these, absorption. Absorption is a function of composition of the material in which a seismic disturbance is propagating and indicates inelastic effects are operating within the material. Through absorption, the energy of a travelling wave is ultimately transferred completely to the propagation meterial in the form of heat, resulting in disappearance of the wave motion. If the effect of absorption can be measured accurately, and the additional quantities listed above accounted for, then the value obtained for the absorption could be used to identify the propagation material. Conversely, knowing the material composition establishes the absorption factor and provides a valuable constraint in various seismic investigations. This is the value of obtaining a sound theoretical and experimental understanding of the variation of absorption

with composition of propagation material.

A large number of interrelated quantities have been used to describe the degree of absorption. The most common of these is the quality factor, Q. It expresses the sharpness of resonance of a mechanical system and is defined by,

$$\frac{1}{Q} = \frac{2\Delta f}{f_n} \qquad (1)$$

where f_n is the natural frequency of the system (see Figure 1).

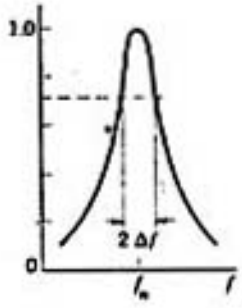

Figure 1. Amplitude vs. frequency response for a mechanical system showing the parameters used in the definition of Q. (from White, 1965)

The quality factor may also be expressed,

$$\frac{2\pi}{Q} = \frac{\Delta W}{W} \quad , \qquad (2)$$

where $\Delta W/W$ is the fractional strain energy loss per stress cycle. Other expressions for Q include,

$$\frac{\pi}{Q} = \delta = V\frac{\alpha}{f} \quad , \qquad (3)$$

where V is the velocity of the wave in the propagating medium, α is the absorption coefficient and f is the frequency of the wave. The quantity δ is the logarithmic decrement and may be defined by,

$$\delta = \ln \frac{A_2}{A_1} \quad , \qquad (4)$$

where A_1 is wave amplitude and A_2 is the amplitude one cycle later. Another common expression is the absorption coefficient, given by,

$$A_1 = A\, e^{-\alpha x} \quad , \tag{5}$$

where A and A_1 are the values of wave amplitude separated a distance, x. The absorption coefficient is α. In addition to these definitions other measures of attenuation are given by a and θ. The quantity, a, is simply referred to as attenuation and is given by,

$$\frac{a}{\pi f} = \frac{1}{Q} \quad , \tag{6}$$

or,

$$\frac{a}{f} = \delta \quad . \tag{7}$$

The factor θ is the phase angle between stress and strain and is,

$$\theta = \frac{1}{Q} \quad . \tag{8}$$

Useful combinations of the above equations include,

$$\delta = \pi\theta \quad , \tag{9}$$

$$\theta = \frac{a}{\pi f} \quad , \tag{10}$$

and,

$$\frac{\Delta W}{W} = 2\pi\theta \quad . \tag{11}$$

These are the quantities most commonly used in the literature to describe absorption. The parameter Q has tended to be utilized most frequently, however the logarithmic decrement, δ, facilitates comparison between different experiments and wave types (body and surface) better as it expresses a general loss observable in a wide range of phenomena. That is, amplitude loss per wavelength, expressed by δ, is readily

applied to any travelling wave. Thus, whenever possible, the various degrees of absorption will attempt to be stated in terms of Q or δ.

Loss Mechanisms and Experimental Results

Loss mechanisms may generally be classified into five groups (1) solid friction losses (intergranular sliding, sticking and sliding), (2) viscous losses (primarily associated with fluids, in this paper), (3) losses due to motion of a fluid in matrix pore space, (4) thermo-elastic losses, and (5) non-linear loss theory. To some degree, absorption in shallow crustal materials is probably a function of all these effects, as well as overburden pressure.

Solid friction and viscous losses are the best understood and have been investigated most thoroughly. They probably explain most of the absorption observed in the shallow crust. Figure 2 shows a stress-strain diagram for solid and viscous losses. For viscous losses, the plot is an ellipse whose area represents the energy lost per cycle. This loss is proportional to the cyclic stress frequency. For very low frequencies, the energy loss per cycle approaches zero and the ellipse degenerates to a straight

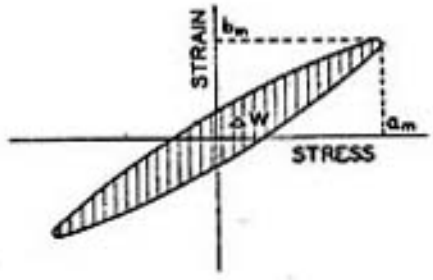

Figure 2. Stress-strain diagram, a_m is maximum stress, b_m is maximum displacement. (from Born, 1941)

line. If absorption is due to solid friction alone, the area of the

ellipse is independent of frequency and depends only on composition of the propagation material and the maximum strain amplitude. Thus, in the case of solid friction losses alone, δ is independent of frequency, while δ is proportional to the first power of frequency for viscous losses. Born (1941) has investigated the effects of frequency on δ for a dry and partially saturated sandstone. He used a resonant bar experimental procedure on an Amherst sandstone for a frequency range of approximately 500 to 3900 Hz. His results are summarized in Figure 3.

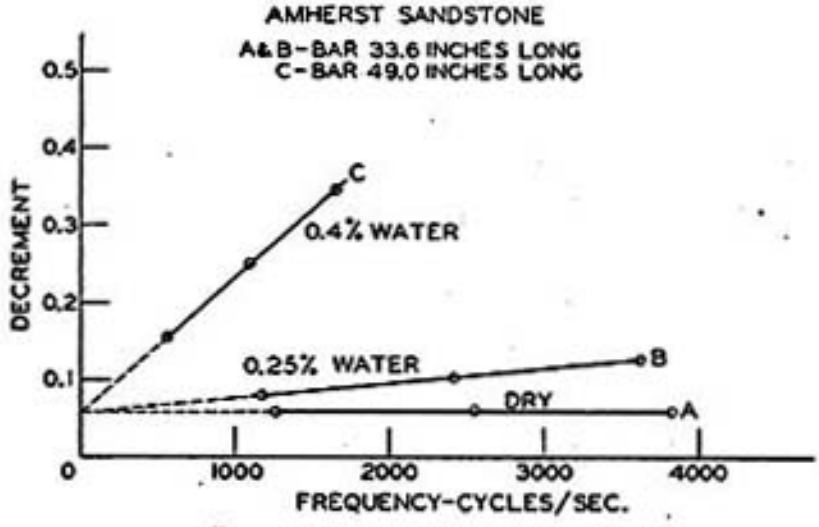

Figure 3. Decrement vs. frequency for dry and saturated Amherst Sandstone samples. (from Born, 1941)

The logarithmic decrement, δ, was found to be essentially independent of frequency for the dry specimen but varied linearly with frequency for various water saturations. These results indicate that the observed decrement is a function of both solid friction and viscous losses, primarily solid friction at low frequencies.

Knopoff and MacDonald (1958) reviewed experimental data on the dissipation of energy in rock-forming materials over the frequency range 10^{-2} to 10^{6} Hz. and found that 1/Q was practically constant. This

observation also implies a solid friction loss mechanism for these materials at surface temperature and pressure. Knopoff and MacDonald (1960) also proposed a macroscopic model for the attenuation of small amplitude stress waves in solids in which solid friction varies as the gradient of local stress. They illustrated the model with a mass-spring system sliding on a rough surface in which the roughness of the surface increases in the direction the mass is moving. They found Q for the model to be independent of frequency. In addition, they cite experimental evidence which indicates a Q dependence on grain surface area in silicate aggregates. Both these observations suggest validity of the solid friction loss mechanism.

There is a large amount of experimental evidence for shallow crustal materials indicating that solid friction losses are of primary importance as an absorptive mechanism while viscous losses are much less a factor. Bruckshaw and Mahanta (1954) determined the variation of Young's Modulus, E, and fractional energy loss per cycle ($\Delta W/W$), with frequency in the range 40 to 120 Hz. They used rock specimens in the form of beams and set the system into forced vibrations. Their results are summarized in Figures 4 and 5. The plots are relatively constant over much of the frequency range, but deviate from linearity somewhat towards the lower frequencies, indicating a loss mechanism occurring which is not strictly of a linear, or solid friction, type. They found the greatest energy losses in the softer, less compacted and poorly indurated rocks. In particular, the value of $\Delta W/W$ for the sandstone seems high.

Usher (1967) performed a similar series of experiments for small beam-shaped rock samples over a frequency range of 2 to 40 Hz. His results are shown in Figures 6, 7 and 8.

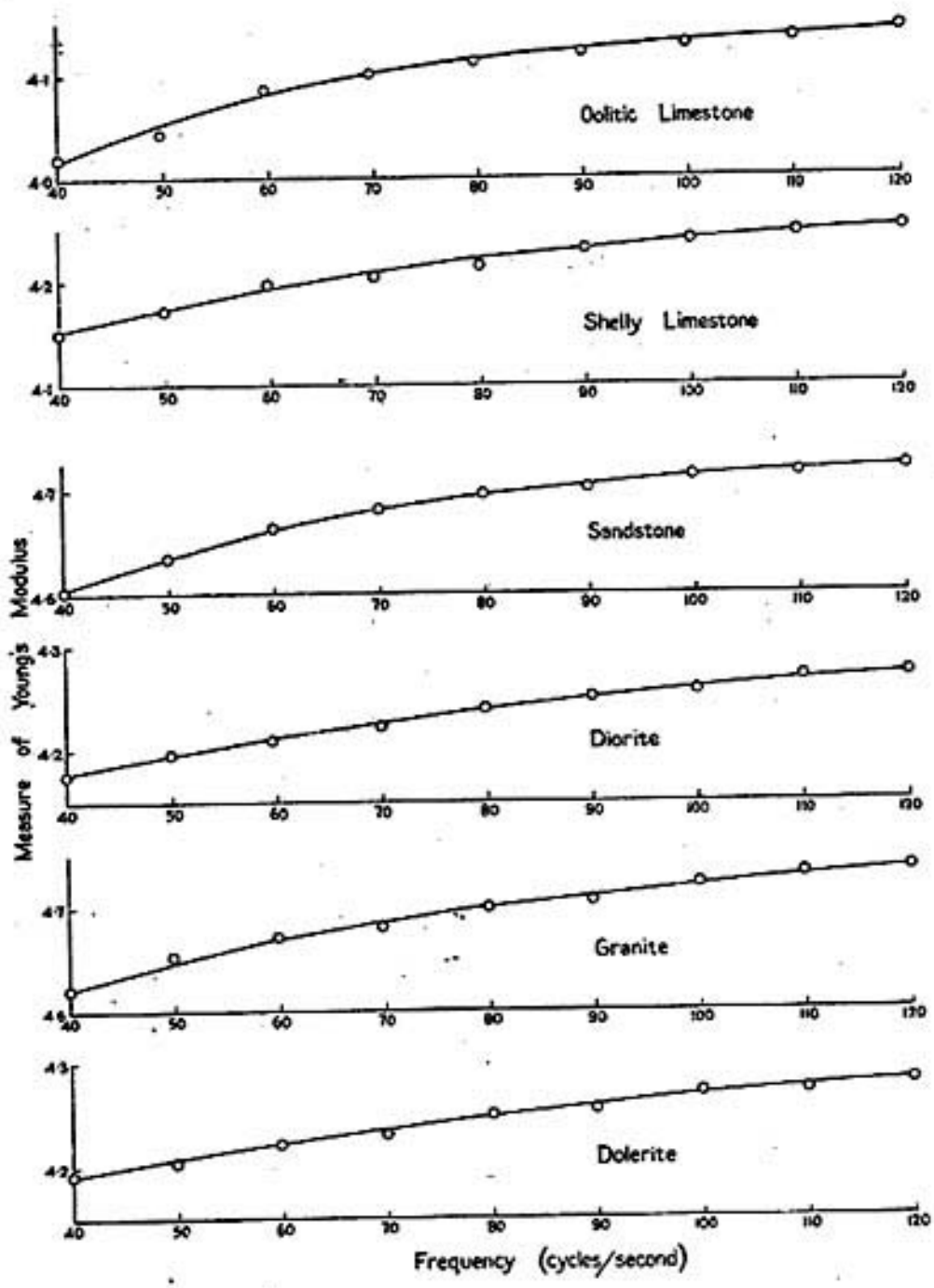

Figure 4. Young's Modulus versus frequency.(from Bruckshaw and Mahanta, 1954)

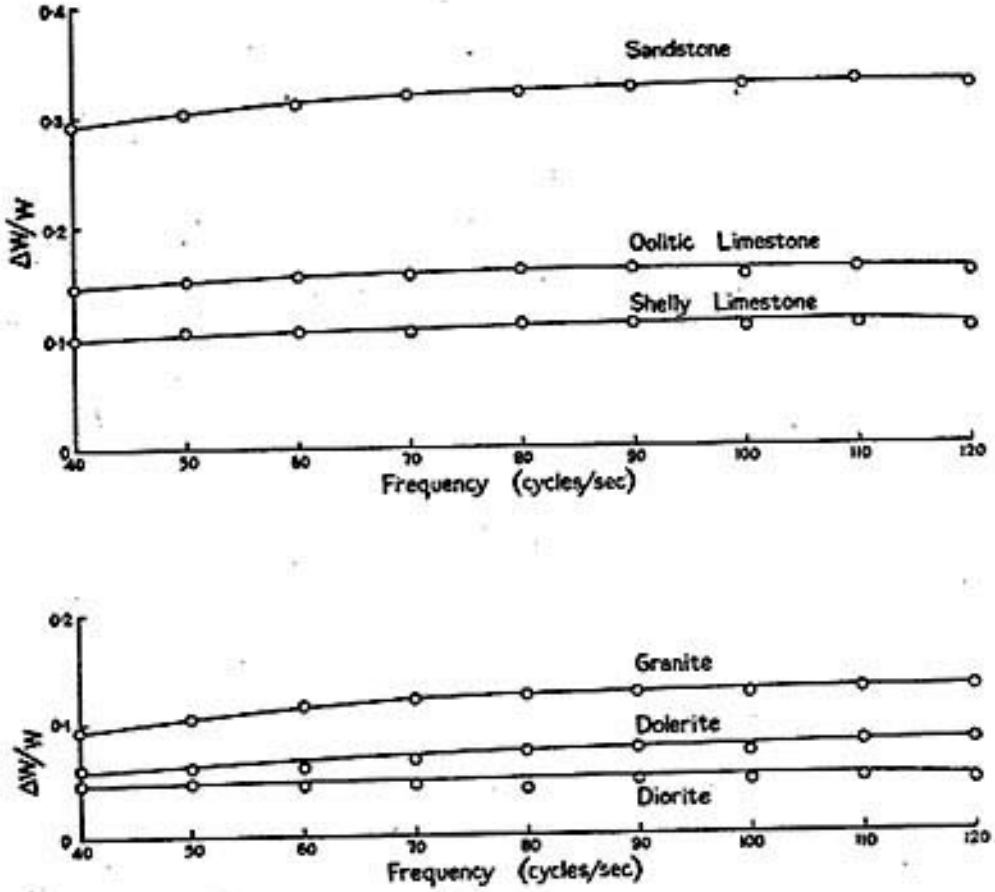

Figure 5. Fractional energy lost per cycle versus frequency.(from Bruckshaw and Mahanta, 1954)

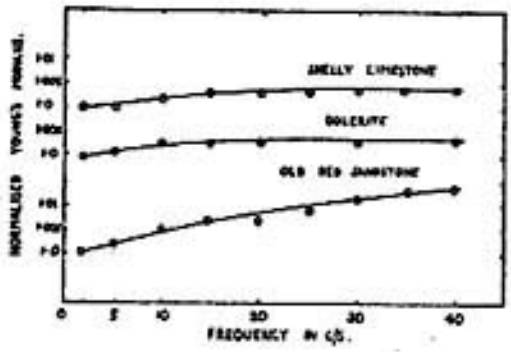

Figure 6. Young's Modulus versus Frequency. (from Usher, 1967)

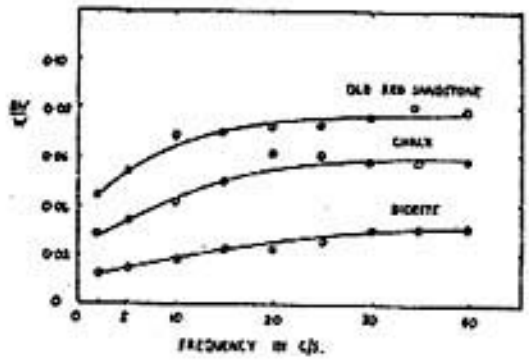

Figure 7. Energy Loss versus Frequency. (from Usher, 1967)

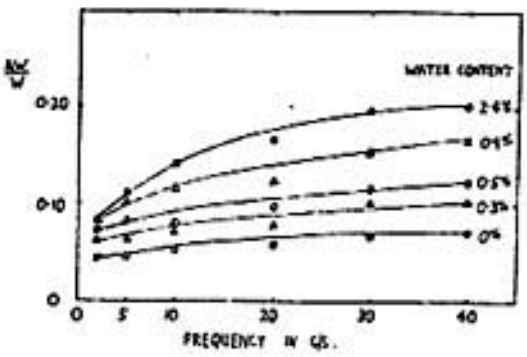

Figure 8. Effect of water content on energy loss as a function of frequency. (from Usher, 1967)

These plots, as do Born's (1941), clearly show the dominant effects of solid friction, with viscous losses becoming more important at lower frequencies and higher percentages of water content. When fluid is forced from compressed to dilated regions energy is dissipated by viscous

means such that $\Delta W/W$ increases with frequency. Usher suggests modifying Knopoff and MacDonald's (1960) model of pure solid friction grain boundary slipping to include viscous slipping at lower frequencies, but pure solid friction at higher frequencies. Usher also points out that the trends seen in Figures 6 through 8 may not be as drastic for rocks in situ, due to increased hydrostatic pressure.

Horton (1959) formulated a loss mechanism for the Pierre shale in terms of a modified Kelvin solid. The model he used is shown in Figure 9. He then compared α (attenuation coefficient) versus frequency curves, calculated using the model, with experimental data obtained by McDonal, et al. (1958) for the Pierre shale. The results for shear waves are presented in Figure 10 and those for compressional waves in Figure 11. The theoretical and experimental data agree well for most parts of the curves and indicate that the model is a good approximation to the actual loss mechanism in the Pierre Shale. McDonal et al. (1958) obtained a value of $\alpha = 0.12\ f$ (db/1000 ft.) from Figure 11 and $\alpha = 1.05\ f$ from Figure 10. Figure 11 applies to vertically-travelling compressional waves over the frequency range 50 to 450 Hz., while Figure 10 includes data from horizontally-travelling shear waves with vertical motion in the frequency range 20 to 120 Hz.

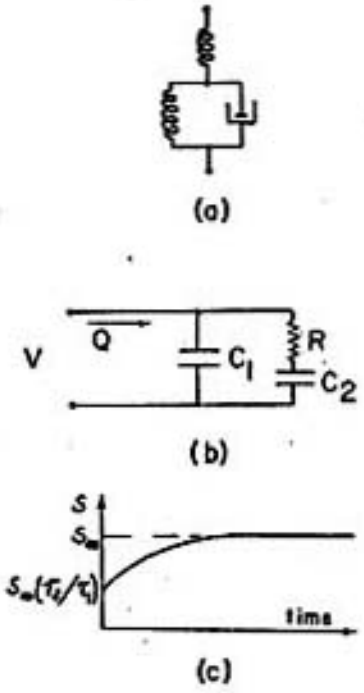

Figure 9. Modified Kelvin solid. (from Horton, 1959)

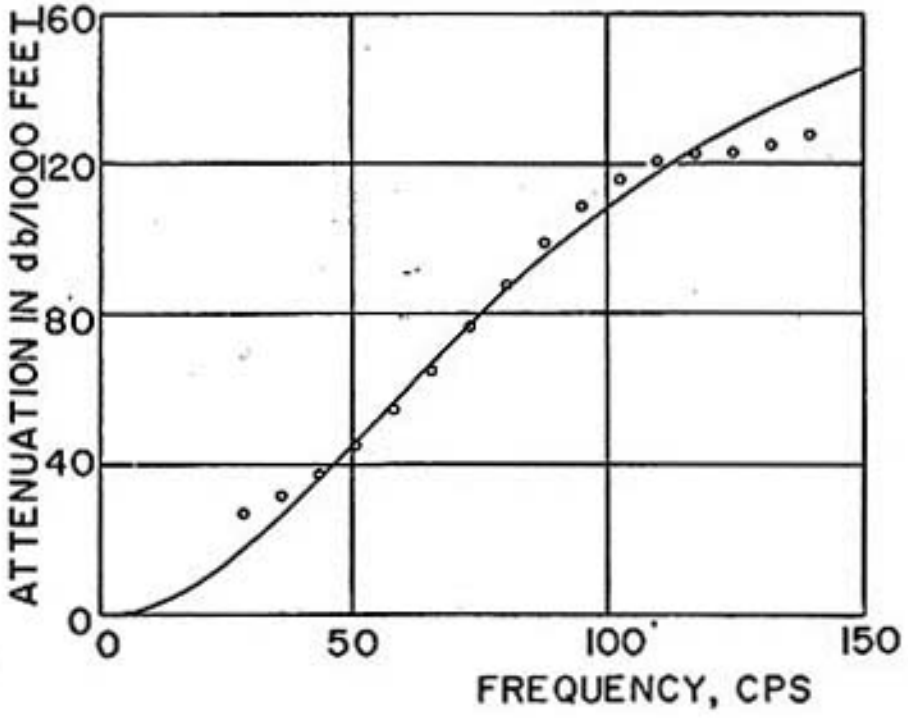

Figure 10. Attenuation of shear waves versus frequency. The solid curve is calculated from theory. (from Horton, 1959)

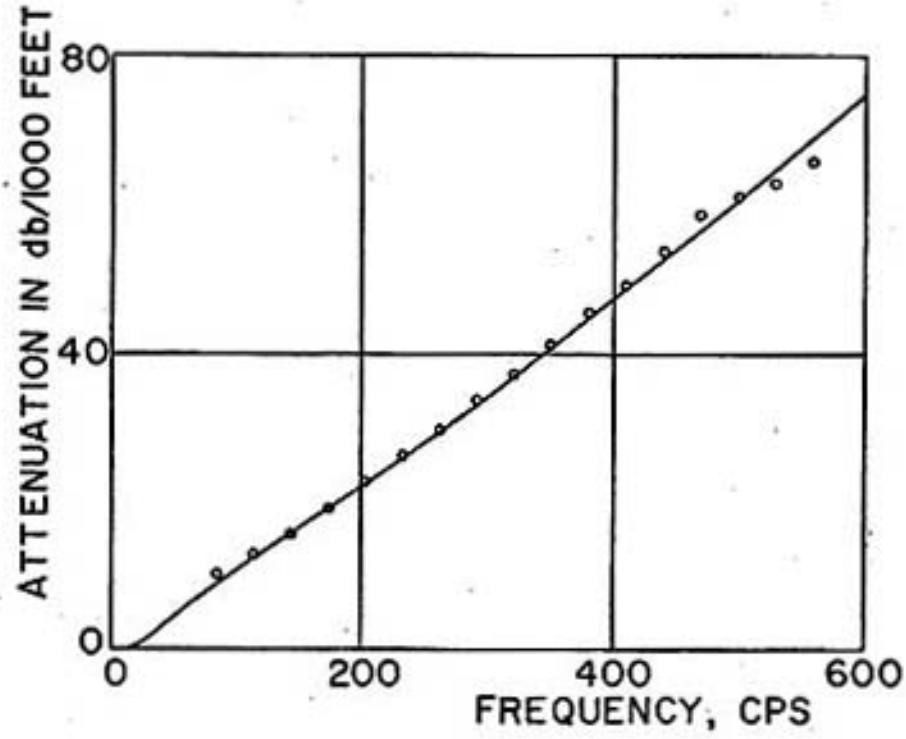

Figure 11. Attenuation of compressional waves versus frequency. The solid curve is calculated from theory. (from Horton, 1959)

Peselnick and Outerbridge (1961) performed a torsion pendulum experiment at room temperature on the Solenhofen Limestone over a frequency range from 4 Hz to 10 MHz to determine internal friction in shear, and shear modulus. They found the shear modulus to be constant within ± 2 percent, at 2.64×10^{11} dynes/cm^2, over the entire frequency range. The results obtained for the logarithmic decrement, δ, are presented in Table 1.

Table 1. Solenhofen Limestone Data
(from Peselnick and Outerbridge, 1961)

Sample	Density, g/cm³	Frequency, cps	Rigidity Modulus, dynes/cm²	Shear Velocity, km/s	Logarithmic Decrement, δ	Remarks
B	2.67	3.89	2.58×10^{11}	3.1	$3.4\text{–}4.1 \times 10^{-3}$	(a)
A	2.67	6.52	2.59	3.1	4×10^{-3}	(b)
C	2.67	8,200	2.66	3.15	5	(c)
C	2.67	16,400	2.66	3.15	5	(c)
B	2.67	9,500	2.68	3.17	5	(c)
B	2.67	18,600	2.61	3.12	5	(c)
B	2.67	28,500	2.69	3.18	...	(c)
S-25	2.66	10×10^6	2.6	3.1	...	(d)
S-1	2.59	9×10^6	2.2	2.9	17	(d)

(a) 7.2 kg/cm² axial tension; maximum shear strain $\sim 7 \times 10^{-6}$ (precision in $\delta = \pm 5$ per cent).
(b) 4.3 kg/cm² axial compression; maximum shear strain $\sim 5 \times 10^{-6}$ (precision in $\delta = \pm 5$ per cent).
(c) Bar resonance technique (precision in $\delta = \pm 10$ per cent).
(d) Pulse-echo technique (precision in $\delta = \pm 15$ per cent).

These results also indicate a solid-hysteresis behavior acting predominantly as a loss mechanism. A possible cause was discussed above in the review of Knopoff and MacDonald's (1960) work.

An interesting compilation of data from a variety of authors and experimental methods has been made by Attewell and Ramana (1966). Their results are summarized in Figure 12.

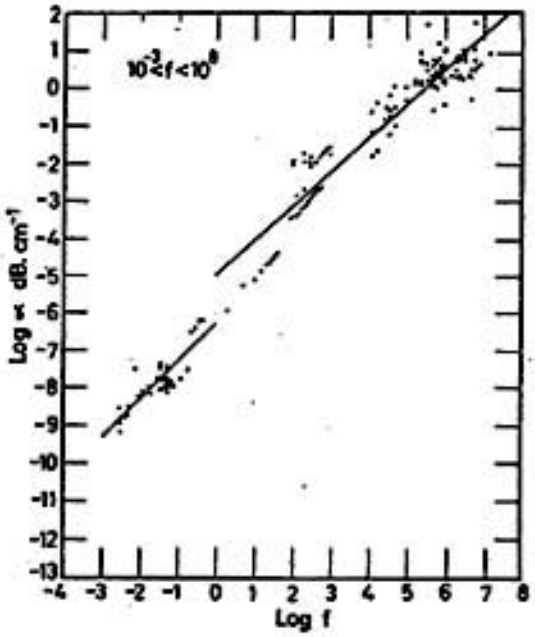

Figure 12. Attenuation coefficient versus frequency for a wide variety of authors and experiments. (from Attewell and Ramana, 1966)

From 26 authors, representing 168 points, they determined the following value for the absorption coefficient,

$$\alpha = 1.99 \times 10^{-6} f^{1.0386} \text{ db/cm} ,$$

for a frequency range of 10^{-3} to 10^{8} Hz. This implies a Q which is practically independent of frequency, supporting the general arguments concerning solid friction losses discussed above.

Figure 13 shows a less inclusive but similar set of data compiled by Hamilton (1972). He worked with saturated marine sediments but concluded that intergrain friction appears to be the dominant cause of wave energy damping. As can be seen from Figure 13, α appears to depend on the first power of frequency and thus Q is independent of frequency. The line marked A in Figure 13 is the result of data collected for sedimentary land strata at relatively low frequencies.

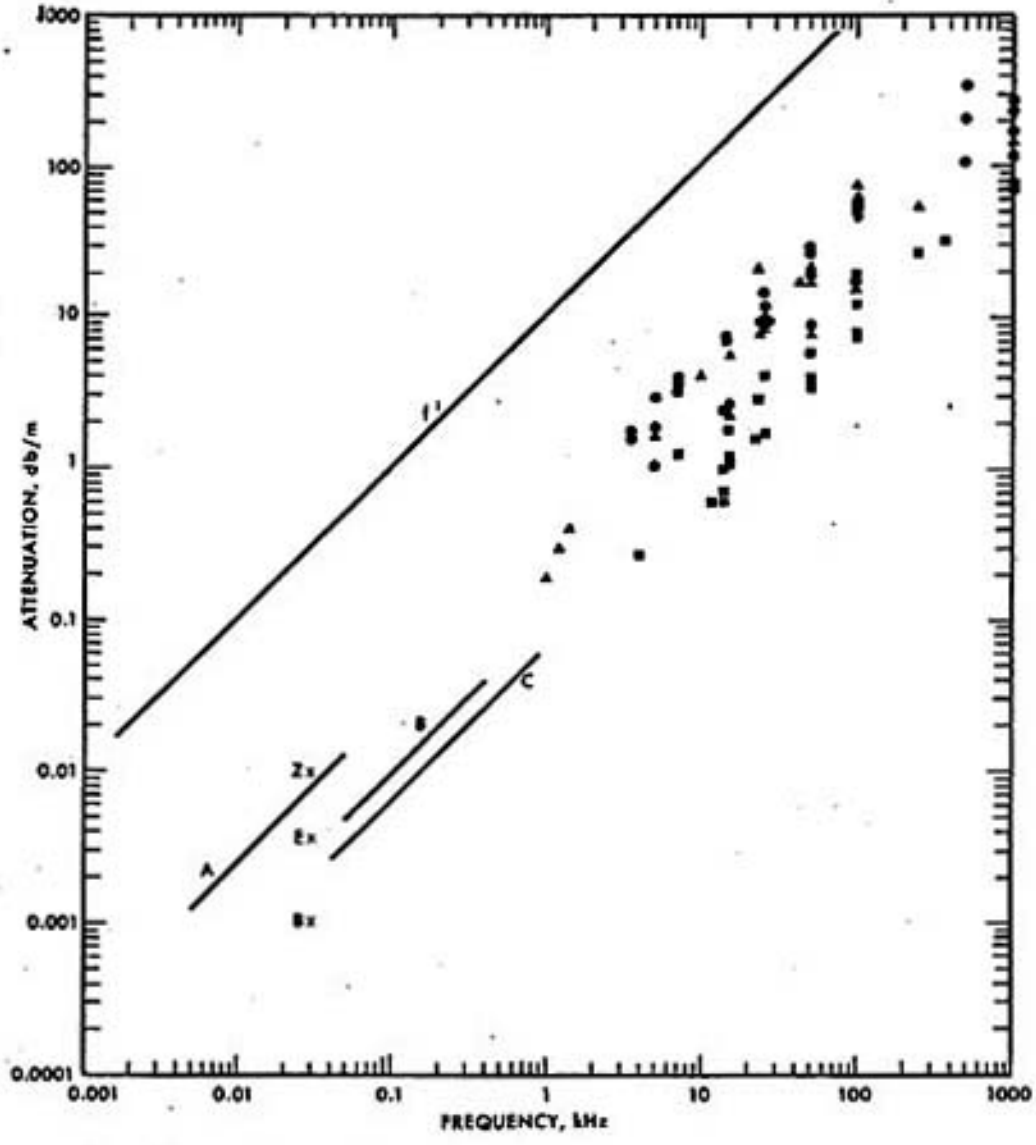

Attenuation versus frequency in natural, saturated sediments and sedimentary strata; data from Tables 1-4b. Symbols: circles-sands (all grades); squares-clayey silt, silty clay; triangles-mixed sizes (e.g., silty sand, sandy silt, sand-silt-clay); sand data at 500 and 1000 khz from Busby and Richardson (1957). Low-frequency data: line A-Zemstov, 1969 (land, sedimentary strata); B-Tullos and Reid, 1969 (Gulf of Mexico coastal clay-sand); C-Bennett, 1967 (sea floor, reflection technique); Z-Zhadin (in Vasil'ev and Gurevich, 1962); E and B-Epinatyeva et al, and Berzon (in Zemstov, 1969). Line labelled f^1 indicates slope of any line having a dependence of attenuation on the first power of frequency.

Figure 13. Compiled attenuation versus frequency. (from Hamilton, 1972)

The third type of loss mechanism is that due to the motion of fluid in pore space relative to the rock matrix. White (1965) has reviewed this mechanism which has been treated in detail by Biot. White utilized

Biot's results by substituting typical values for rock and fluid into Biot's equations for a_p and a_s, attenuation of compressional and shear waves, respectively. This resulted in values of,

$$a_p = 9 \times 10^{-12} f^2 \text{ sec}^2/\text{cm},$$

and,

$$a_s = 65 \times 10^{-12} f^2 \text{ sec}^2/\text{cm}.$$

These values should be valid to frequencies of approximately 20,000 Hz (White, 1965). However, for frequencies of interest in seismology and seismic prospecting (< 100 Hz), the values obtained for a_p and a_s are so much lower than typically measured values, that absorption due to this mechanism is probably insignificant (White, 1965).

Hamilton (1972), in his study of attenuation of compressional waves in saturated marine sediments, also concluded that viscous losses, due to the relative movement of pore water and mineral structure, are negligible. Thus, for the frequencies of interest in this paper, the absorptive losses due to this type of mechanism will not be considered important.

The fourth type of loss mechanism to consider is that due to thermoelastic effects. Since all real materials have a finite thermal conductivity, stress waves propagating through such material will lose energy due to heat conduction. Treitel (1959) has derived equations of motion and temperature for an elastic solid with a finite thermal conductivity using the irreversible form of the second law of thermodynamics. He obtained the following expression for the absorption coefficient,

$$\alpha = \frac{1}{8} \frac{K w^2}{V_p^3}, \qquad (12)$$

where K is thermal diffusivity, w is angular frequency ($w = 2\pi f$) and V_p is compressional wave velocity. This expression implies a Q which varies as the first power of frequency. In this respect, this mechanism produces the same type of frequency dependent Q as the viscous loss mechanism. Figure 14 is a plot of the results of equation (12) using the following values,

copper: $w << 1.8 \times 10^{11}$ rad/sec
$K = 1.14$ cm^2/sec
$V_p = 4.6 \times 10^5$ cm/sec

rock: $w << 2.5 \times 10^{13}$ rad/sec
$K = 0.01$ cm^2/sec
$V_p = 5 \times 10^5$ cm/sec .

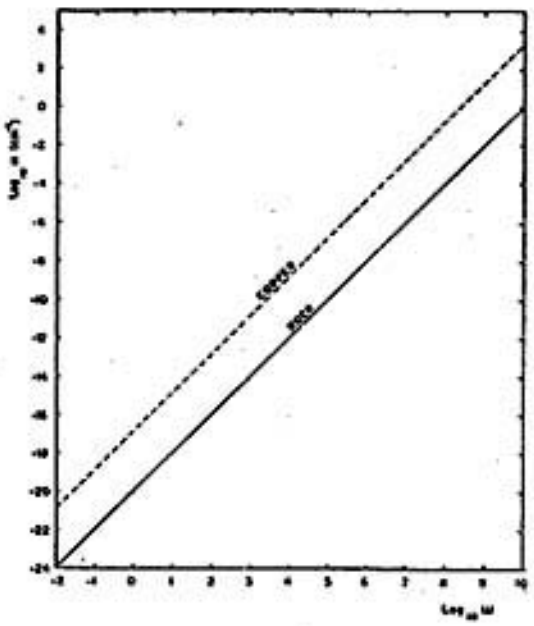

Figure 14. α versus circular frequency for copper and rock with the properties described above. (from Treitel, 1959)

The last loss mechanism to be considered is non-linear processes. A nonlinear mechanism for absorption was initially proposed primarily to account for the observation that the Q spectrum for many solids

appeared to be flat (α depends precisely on the first power of frequency). Collins and Lee (1956), though, showed that by assuming a variation of α with f^{1+n}, where n is a very small number, a strictly linear theory could be applied. There is a large amount of evidence, some of which has been reviewed above, that the Q spectrum is not completely flat. Thus Collins and Lee's assumption appears to be experimentally valid. Several linear mechanisms have been proposed and discussed above which adequately describe the Q spectrum within the limits of the calculated Q responses, using the f^{1+n} assumption. It has also been pointed out by Savage and Hasegawa (1967) that a nonlinear mechanism should produce a cusping, or sharpening, of seismic pulses. Yet it is observed that seismic pulses are broadened, and cusps smoothed during transmission through shallow, crustal materials. Thus, it is not necessary to introduce the added complications of nonlinear loss theory.

Discussion

The primary result from the above observations is that absorptive loss in shallow crustal materials is mainly attributable to solid friction, in which Q is approximately independent of frequency. The slight observed deviations from this relation may be explained by losses due to either a viscous or thermoelastic mechanism. Losses of these latter two types produces a Q which varies approximately as the first power of frequency.

Various values of δ, α and Q, as determined experimentally above, can be used to give a rough indication of the average value of Q likely to be observed in near-surface crustal materials. A summary of various experimenters' results, which includes many of the works cited above, has been presented in Figure 12. Attewell and Ramana (1966) have calculated

an average Q for this data of,

$$\overline{Q} = 213f^{-0.015}, \quad 10^{-3} < f < 10^{7}.$$

The size of the exponent indicates that Q is practically independent of frequency. This value is probably too low for crustal material in situ. The pressure of overburden will substantially raise Q. Båth (1973) indicates a Q for the crust of approximately 470, while Press (1964) determined Q, from underground nuclear explosions in Nevada, to be 260 ± 40. Thus a value around 300 may be more typical of crustal material in situ.

Assuming the effect of overburden pressure has an equal effect on Q_α and Q_β (Q for compressional and shear waves, respectively), a calculation of the ratio Q_α/Q_β can be made for absorption data taken at relatively shallow depths in the field. A study, discussed above, particularly useful in this regard is the determination of absorption for compressional and shear waves in the Pierre Shale, performed by McDonal et al. (1958). A summary of their results is presented by Bradley and Fort (Clark, 1966) and is reproduced in Table 2, after conversion to Q from percent energy lost per cycle. In calculating average values for Q_α and Q_β, and forming their ratio, the effects of the frequency at which the measurements were taken was not considered.

Table 2. Q_α and Q_β for the Pierre Shale

Q_α	Q_β
31.4	11.5
37.8	11.4
37.4	12.4
38.6	12.0
36.1	9.1
36.9	9.4
33.4	10.4
34.3	11.1
36.4	

The justification for this has already been established in the discussion above. Average values for the compressional and shear quality factors are,

$$\overline{Q}_\alpha = 35.8 \text{ and } \overline{Q}_\beta = 10.9 \ .$$

The ratio $Q_\alpha/Q_\beta = 3.28$. The measurements leading to these results were performed on the Pierre Shale, a formation known for its' homogeneous and isotropic nature, at depths ranging from 260 to 750 feet. Should this Q_α/Q_β for the Pierre Shale be considered a reasonable result applicable to different rock types at different depths? Bremaecker et al. (1966) measured similar data on an aa lava flow, unconsolidated cinders, and compact limestone, at the surface. By assuming a complex shear modulus but a real λ (Lamé constant) they determined a relation for Q_α/Q_β

$$Q_\alpha/Q_\beta = 0.5\ \alpha^2/\beta^2 \ , \qquad (13)$$

where α is compressional velocity and β is shear velocity. The justifications for the assumptions leading to equation (13) first start with the statement that imperfect elasticity can be expressed by making both μ (shear modulus) and λ complex. However, for sedimentary rocks, λ' (complex Lamé constant) approaches zero, resulting in equation (13) (De Bremaecker et al., 1966).

Now consider the values for α and β as determined by McDonal et al. (1958) for the Pierre Shale: $\alpha = 7100$ ft/sec, $\beta = 2630$ ft/sec. Substitution into equation (13) yields:

$$Q_\alpha/Q_\beta = 3.64 \ .$$

This should be compared with the ratio calculated from Table 2 of $Q_\alpha/Q_\beta = 3.28$. Considering the great range of environments, experimental conditions, and the assumption of equal overburden pressure effect on Q_α and Q_β, the

values are remarkably close. This suggests that equation (13) could have rather general applications to a wide range of rock types and depths of burial.

An attempt can now be made to obtain the ratio Q_α/Q_β for shallow (<20 km) crustal materials in the Socorro area by using equation (13). The values for compressional and shear wave velocities commonly used in this area are: α = 5.80 km/sec and β = 3.35 km/sec. Substitution into equation (13) yields Q_α/Q_β = 1.50. This value is considerably lower than the one obtained above for the Pierre Shale. The difference is probably the result of using body waves which have traversed a volume of deeper rock and thus greater overburden pressure. In near surface, unconsolidated rock, one might expect the shear wave to be affected to a greater extent than the compressional wave. This difference would tend to diminish as the waves reached better indurated rock at higher confining pressure. This is reflected in the lowering of the ratio Q_α/Q_β.

This value for Q_α/Q_β of 1.50 for the Socorro area can now be used to help indicate whether calculating the ratio, by using the dominant frequencies of P and S waves, is valid. The proposed relation is,

$$Q_\alpha/Q_\beta = \nu_\alpha/\nu_\beta \quad , \tag{14}$$

where ν_α and ν_β are the dominant frequencies of the P and S waves, respectively. These values have been determined to be ν_α = 19.7 ± 1.5 Hz and ν_β = 12.3 ± 0.3 Hz using a zero-cross counting technique for a group of 15 randomly selected microearthquake events. Thus ν_α/ν_β = 1.60. This value, considering the standard deviations for ν_α and ν_β, is within the range of the ratio Q_α/Q_β = 1.50 obtained with equation (13), indicating that equation (14) may be approximately valid.

The basic assumptions used in these determinations of Q have been (1) Q is independent of frequency, (2) the loss mechanism is primarily of the solid friction type, and (3) observed absorption is an approximately linear process. These assumptions have been justified in the preceeding discussion.

Conclusions

It is well known that shear waves are less efficiently transmitted in bulk, in situ, crustal materials, than P waves. The value of Q_α/Q_β = 1.60 obtained above reinforces this belief. If values calculated in this manner can be believed, and if the ratio varies with rock type, Q_α/Q_β could be used to determine the average composition of material through which a seismic disturbance propagates. By performing field experiments in which travel paths from seismic sources are plotted and have individual, calculated Q_α/Q_β ratios associated with them, volumes of crust might be defined which exhibit a particular value of the ratio. Ratios for different volumes could then be compared and relative material properties assigned to each volume. If relatively unique ratios can be found, or determined experimentally, for particular material compositions, then the rock types in these regions could be approximately identified. The effects of different depths of burial would have to be accounted for, but the correction could become rather small below a certain critical depth and above 20 km, such that the total variation of Q_α/Q_β with overburden pressure could be insignificant in this range (critical depth to 20 km). In addition, by using equation (13), relative velocities could be assigned to these crustal volumes and thus aid in determining a velocity model. This could be particularly valuable in an area which is geologically complex and does not readily conform to a model consisting of homogeneous

layers.

The approximate spatial variation of the ratio Q_α/Q_β, as determined by travel path plotting, can thus be a valuable constraint in the formulation of earth models of the shallow crust.

References

Attewell, P. B., and Ramana, Y. V., Wave Attenuation and Internal Friction as Functions of Frequency in Rocks, Geophysics, 31, pp. 1049-1056, 1966.

Båth, Markus, Introduction to Seismology, Birkhauser Verlag Basel and Stuttgart, Stockholm, 1973.

Born, W. I., The attenuation Constant of Earth Materials, Geophysics, 6, pp. 132-148, 1941.

Bruckshaw, J. McG., Mahanta, P. C., The Variation of the Elastic Constants of Rocks with Frequency, Petroleum, 17, pp. 14-18, 1954.

Clark, Sydney P. (editor), Handbook of Physical Constants, The Geological Society of America, Inc., New York, 1966.

Collins, Francis, and Lee, C. C., Seismic Wave Attenuation Characteristics from Pulse Experiments, Geophysics, 21, pp. 16-40, 1956.

DeBremaecker, J. CL., Godson, Richard H., Watkins, Joel S., Attenuation Measurements in the Field, Geophysics, 37, pp. 562-569, 1966.

Hamilton, Edwin L., Compressional-Wave Attenuation in Marine Sediments, Geophysics, 37, pp. 620-646, 1972.

Horton, C. W., A Loss Mechanism for the Pierre Shale, Geophysics, 24, pp. 667-680, 1959.

Knopoff, L., MacDonald, G. J. F., The Attenuation of Small Amplitude Stress Waves in Solids, Revs. Modern Phys., 30, pp. 1178-1192, 1958.

Knopoff, L., MacDonald, G. J. F., Models for Acoustic Loss in Solids, Jour. Geophys. Res., 65, pp. 2191-2197, 1960.

McDonal, F. J., Angona, F. A., Mills, R. L., Sengbush, R. L., Van Nostrand, R. G., White, J. E., Attenuation of Shear and Compressional Waves in

Pierre Shale, Geophysics, 23, pp. 421-439, 1958.

Peselnick, L., Outerbridge, W. F., Internal Friction in Shear and Shear Modulus of Solenhofen Limestone over a Frequency Range of 10^7 Cycles per Second, Jour. Geophys. Res., 66, pp. 581-588, 1961.

Press, F., Seismic Wave Attenuation in the Crust, Jour. Geophys. Res., 69, pp. 4417-4418.

Savage, James C., Hasegawa, Henry S., Evidence for a Linear Attenuation Mechanism, Geophysics, 32, pp. 1003-1014, 1967.

Treitel, Sven, On the Attenuation of Small-Amplitude Plane Stress Waves in a Thermoelastic Solid, Jour. Geophys. Res., 64, pp. 661-665, 1959.

Usher, M. J., Elastic Behavior of Rocks at Low Frequencies, Geophys. Prospecting, 10, pp. 119-127, 1962.

White, J. E., Seismic Waves, radiation, transmission and attenuation, McGraw-Hill Book Company, New York, 1965.